CHAPTER III

UNIVERSALITY OF REENTRANT NEMATIC-SMECTIC C-SMECTIC A AND NEMATIC-SMECTIC A-SMECTIC C MULTICRITICAL POINTS

3.1 INTRODUCTION

The nemaric-smectic A-smectic C multicritical point or NAC point for short, is of considerable current interest. A number of experimental as well as theoretical studies have been carried out to understand the nature of this interesting multicritical point. The scheme of presentation of this chapter is as follows. We shall first define the NAC point and summarise the studies which have shown that the topology of the phase diagram near the NAC point is universal. We shall then describe the observation on a second multicritical point, namely, the reentrant nematic-smectic C-smectic A point (RN-C-A), which shows conclusively that NAC and RN-C-A points exhibit the same universal behaviour.

3.1.1. MAC Multicritical Point

The NAC multicritical point was first theoretically predicted and later found experimentally. When it was initially suggested the two proposed explanations were quite different. Chu and McMillan[1] (CM) proposed a model wherein the order parameter of smectic C was nothing but the dipolar order parameter defined in McMillan's

theory.[2] The order parameter of smectic A phase in their approach was the one dimensional density wave of Kobayashi, McMillan and de Gennes.[3] The tilt of the director away from the layer normal enters this CM model somewhat incidentally through a gradient term coupling the two order parameters. The other theoretical approach due to Chen and Lubensky[4] (CL) expected the NAC point to be a kind of Lifshitz point defined earlier by Hornreich, Luban and Shtrikman[5] for magnetic systems. In the CL model the tilt of the director with respect to the layer normal is the central feature and the NAC point is obtained when the coefficient of transverse gradient term in the Landau-Ginzburg free energy expression becomes negative. The CL model predicted a phase diagram as shown in Fig.3.1.

The CL model makes some important predictions concerning the xray scattering behaviour and also the behaviour of elastic constants. It predicts, (1) that the xray scattering in the nematic phase near the NAC point should have a $q_{\perp}^{-4}$ dependence in the transverse direction rather than the usual $q_{\perp}^{-2}$ behaviour predicted by the CM model, (2) that at the NAC point the elastic constants K_1 and K_2 should diverge as $\ln\xi$ (where ξ is the correlation length for fluctuations of smectic order parameter) while K_3 should diverge as ξ and (3) a fluctuation crossover at the NAC point-the pretransition fluctuations in nematic phase are expected to crossover from smectic A like to smectic C like fluctuations. The first experimental observation of the NAC point was by Johnson et al.[6] Using differential scanning

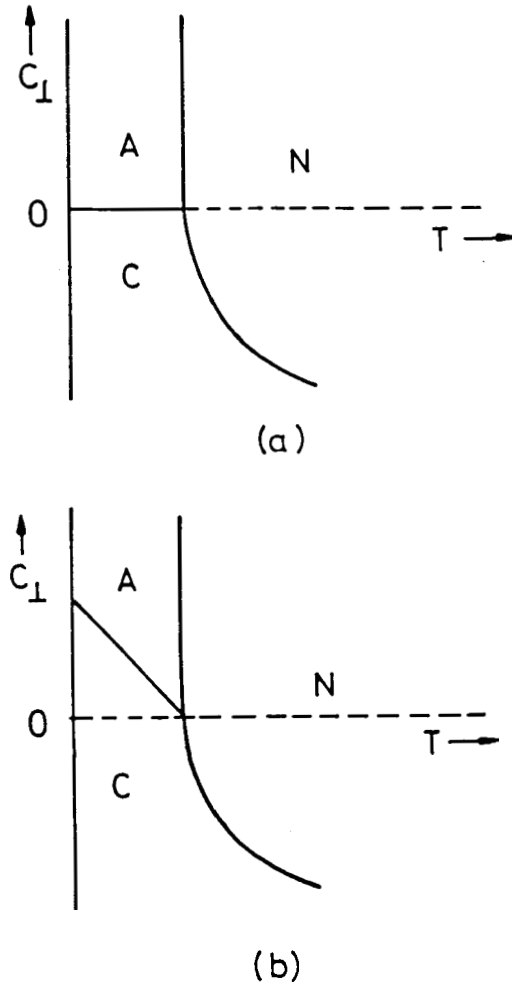

Figure 3.1

Phase diagram of the system showing NAC point predicted by the Chen & Lubensky model. (a) before and (b) after refinement (ref. 4).

calorimetry and thermal microscopy techniques, they reported that the temperature-concentration (T-X) diagram of octyloxy- and heptyloxy-p-pentyl phenyl thiol benzoate (8S5 and 7S5) exhibits a NAC point (Fig. 3.2a). One of these compounds, namely, 8S5 shows nematic, smectic A and smectic C phases, while the other (7S5) shows only nematic and smectic C phases. Addition of 7S5 to 8S5 decreases the srnectic A range and finally for concentrations above 42% of 7S5 (mole %), the nematic phase directly goes to the smectic C phase resulting in a NAC point. Differential scanning calrometry experiments led to the following observations:

a) A-C transitions are continuous and do not show any pretransitional effects.

b) A-N transitions are continuous and show strong pretransitional effects which vanish as the NAC point is approached (Fig. 3.2b)

c) N-C transitions are weakly first order and show very weak pretransitional effects. The NC transition entropy vanishes as the NAC point is approached (Fig. 3.2b).

d) The point where the three phase transition boundaries (NA, NC and AC) meet is a multicritical point. At that point the three phases become indistinguishable.

Johnson et al.[6] also formulated a phenomenological Landau theory to give a qualitative description of the observed phase diagram.

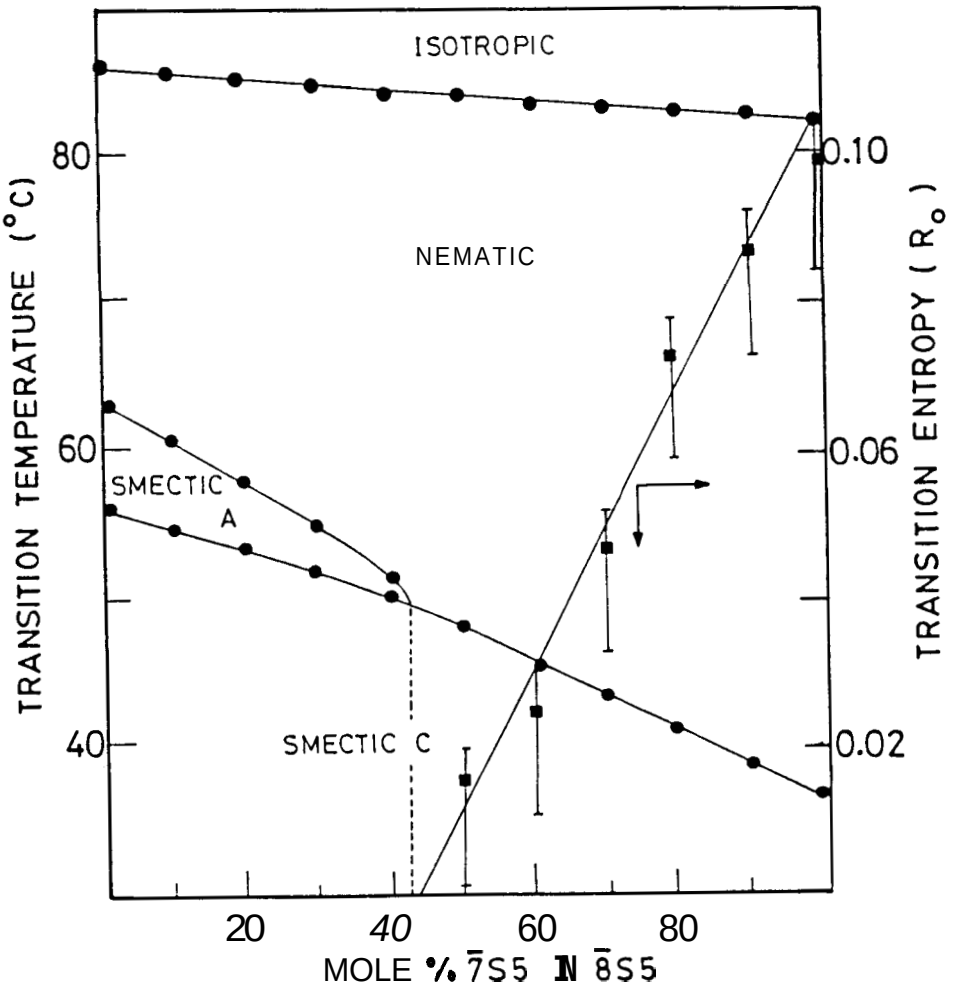

Figure 3.2a

Isobaric temperature-concentration phase diagram of $\bar{8}$S5 and $\bar{7}$S5. Solid circles represent phase transition temperatures. The solid squares represent the NC transition entropy (ref. 6).

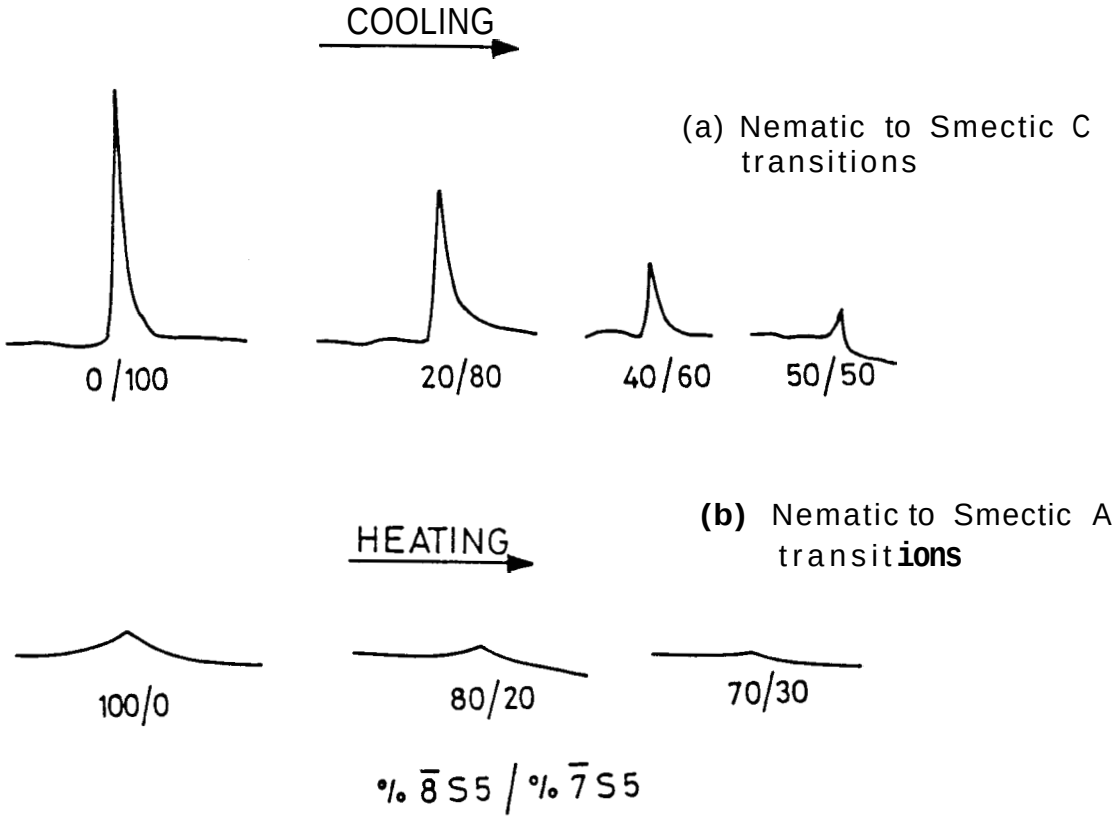

Figure 3.2b

a) DSC traces of the nematic-smectic C transitions of several 8̄S5/7̄S5 mixtures illustrating the rapid decrease of transition entropy as the multicritical point is approached.

b) DSC traces of the nematic-smectic A transitions of several mixtures of 8̄S5 and 7̄S5. The traces show the weakening of the transitions as the multicritical point is approached.

Numbers below the traces indicate the respective concentrations of 8̄S5 and 7̄S5 in the mixtures (ref. 6.).

Sigaud and coworkers[7] independently reported another system, which showed the NAC point, again in the T-X plane. The compounds used were 4'-octyloxy-4-cyanobiphenyl (8OCB) and 2-p-n-heptyloxy amino flurenone (7ONE). The topology of the phase diagram (Fig.3.3) is apparently different from that of Johnson et al.[6] These experiments were followed by accurate high resolution calorimetric[8,9] and xray experiments,[10,11] which permitted explicit comparisons with the theoretical predictions.

Recently, Brisbin et al.[12] have obtained high resolution phase diagrams of four binary liquid crystal systems exhibiting the NAC point (Fig.3.4). It was observed that these four phase diagrams exhibit remarkable topological similarities in the close vicinity of the NAC point. The authors provided quantitative evidence to show that in spite of gross differences in global features universality rules near the NAC point. This was proved by considering relationships between the parameters describing the AN and NC boundaries, viz., the exponent η and the amplitudes A_{NA} and A_{NC}, the parameters being defined by the following expressions,

$$T_{NA} - T_{NAC} = A_{NA}(X_{NA} - X_{NAC})^{\eta} + B(X_{NA} - X_{NAC}) \qquad [1a]$$

$$T_{NC} - T_{NAC} = A_{NC}(X_{NAC} - X_{NC})^{\eta} + B(X_{NAC} - X_{NC}) \qquad [1b]$$

Here X is the mole fraction of the constituent having the smectic A phase. X_{NAC} and T_{NAC} refer to the concentration and temperature

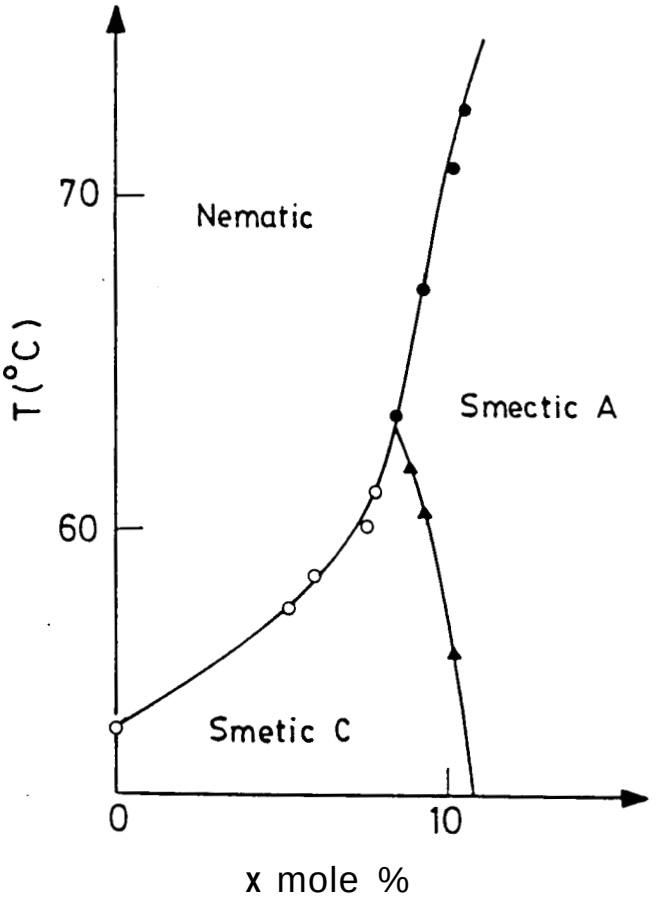

Figure 3.3

Isobaric temperature-concentration phase diagram of 70NE-80CB system (ref. 7).

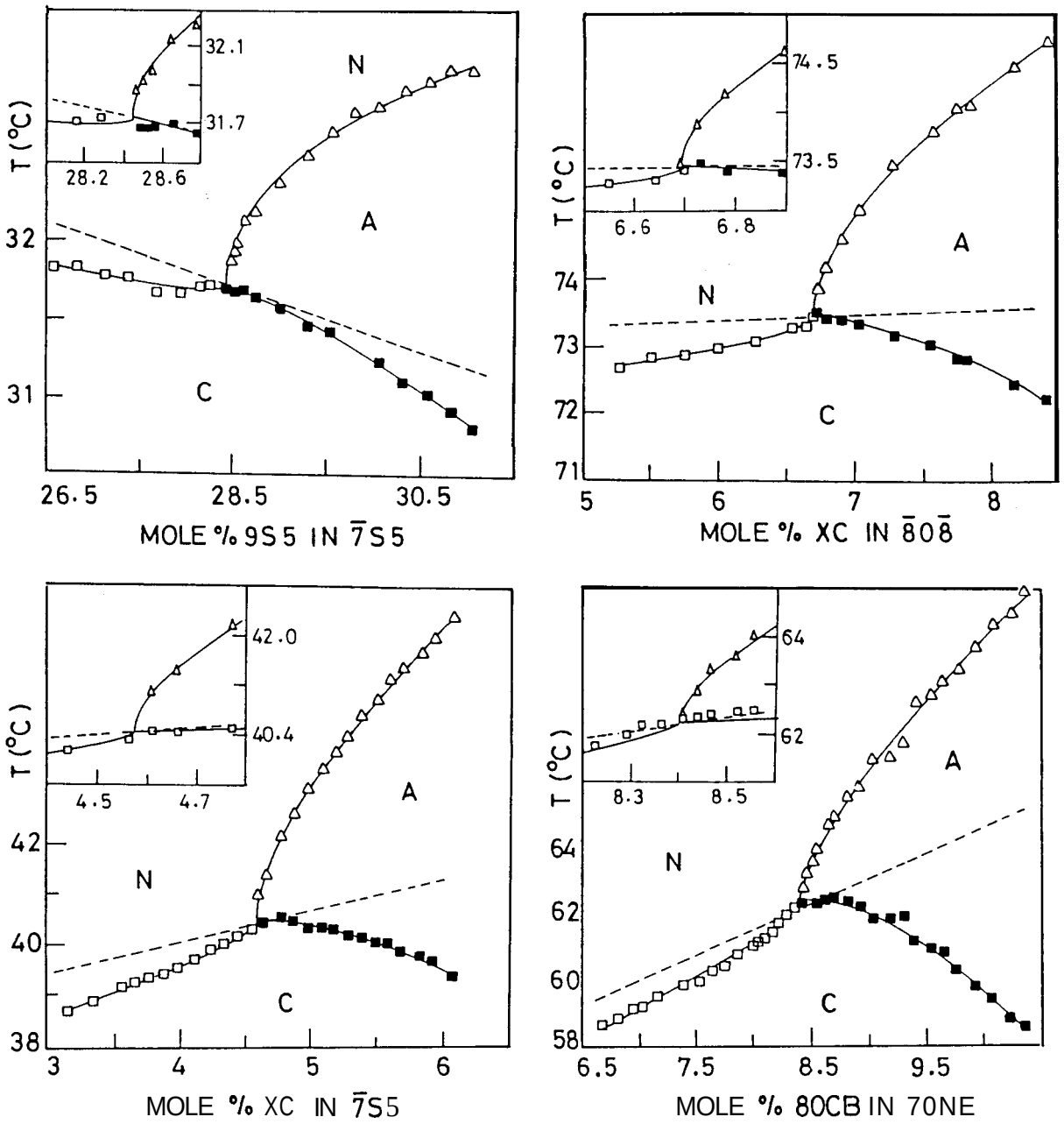

Figure 3.4

High resolution temperature concentration phase diagrams of :

a) 4-n-Pentyl-phenyl thiol-4'-nonylbenzoate (9S5) **and**
4-n-pentyl-phenyl thiol-4'-heptyloxybenzoate (7S5)

b) 4-n-propionyl **phenyl-trans** (4-n-pentyl)cyclohexane **carboxylate (XC) and**
4-n-octyloxy phenyl-4'-n-octyloxy **benzoate (808)**

c) **4-propionylphenytrans** (4-n-pentyl)cyclohexane carboxylate **(XC) and**
4-n-pentyl-pentyl thiol-4'-heptyloxybenzoate (7S5)

d) 4'-octyloxy-4-cyanobiphenyl (8OCB) **and** 2p-n-heptyloxybenzylidene **amino**
flurenone (7ONE).

The inset shows the diagram close to the NAC point (ref. 12).

respectively corresponding to the NAC point.

The results of fitting the data of Brisbin et al. to equations [1a] and [Ib] with and without the universality constraints on η and the amplitude ratio $R = A_{NA}/A_{NC}$ are given in Table 3.1. Solid lines in Fig.3.4 show that fits constrained to have universal values are excellent. Goodness of the fit is objectively indicated by the small increase of χ^2 that accompany the application of universality constraints. Dashed lines in the figures represent the best-fit slope(B) term in equations [1a] and [1b] with the constraints in effect. Solid lines through the AC data represent equations of the form [1a] and [1b] wherein the values B, X_{NAC} and T_{NAC} obtained from the NA/NC fits have been used, along with the constraint that η_{AC} is universal for all the four systems. Again, the fits are very good. Thus Brisbin et al. showed that with a simple choice of the scaling axes, "the NAC diagrams exhibit quantitative unversality".

Since all the studies described so far were on binary systems the need arose to observe the NAC point in a single component liquid crystal system in the pressure-temperature (P-T) plane to test the concept of universality near such a point, since it is unlikely that both density and concentration fluctuations would produce the same topological distortions of the phase diagram. With this in view a series of experiments were conducted by Shashidhar et al. on a number of a systems. Although the initial experiments[13] were unsuccessful,

TABLE 3.1

Best-fit parameters and values of χ^2 for fits of data by equations [1a] and [1b] (see the text for details). Numbers in parentheses correspond to computations carried out excluding the data for 7ONE/8OCB.

$R = A_{NA}/A_{NC}$ (From ref. 12)

	7̄S5/9S5	8̄O8̄/XC	7̄S5/XC	7ONE/8OCB
η		0.573 ± 0.02 (0.556 ± 0.02)		
R		-5.96 ± 1.3 (7.63 ± 2.2)		
A_{NC}	-2.6 ± 0.9 (-1.9 ± 0.7)	-6.9 ± 2.3 (-4.9 ± 2)	-9.4 ± 3.1 -6.6 ± 2.6)	-10.3 ± 3.4
B	-20 ± 4.2 (-18 ± 4)	8 ± 10 (18 ± 10) χ^2 = 1.162(1.00)	63 ± 13.6 (75 ± 13)	157 ± 16
η_{AC}	1.76 ± 0.3 (1.71 ± 0.3)	1.4 ± 0.07 (1.41 ± 0.1) χ^2 = 0.869 (0.914)	1.47 ± 0.04 (1.48 ± 0.04)	1.6 ± 0.04
η_{AC}		1.52 ± 0.03 (1.46 ± 0.03) χ^2 = 0.977 (0.919)		

the NAC point in single component system was indeed observed[14] for 4-n-heptacyl phenyl-4'-(4"-cyanobenzoyloxy)benzoate (7APCBB). The P-T diagram of 7APCBB showing NA, AC and NC transitions up to 600 bars is shown in Fig.3.5. It is seen that all the three boundaries are straight initially but they curl up dramatically as they approach the multicritical point thereby exhibiting pronounced singularities.

Shashidhar et al. improved the resolution of the high pressure set up and obtained high resolution data in the immediate vicinity of the NAC point. These data are shown in Fig.3.6. The universal T-X plot of Johnson[15] is shown in Fig.3.7 for comparison where the data for all the four binary systems mentioned earlier have been plotted together after suitable normalization. The striking similarity between the two Figures 3.6 and 3.7 is obvious. Shashidhar et al. demonstrated quantitative similarities by fitting their P-T data for the NA, NC and AC boundaries individually to the following expressions which are similar to those of Brisbin et al.[12] except that P replaces X.

$$T_{NA}-T_{NAC} = A_{NA}(P_{NAC}-P_{NA})^{\eta_{NA}} + B(P_{NAC}-P_{NA}) \qquad [2a]$$

$$T_{NC}-T_{NAC} = A_{NC}(P_{NC}-P_{NAC})^{\eta_{NC}} + B(P_{NC}-P_{NAC}) \qquad [2b]$$

$$T_{AC}-T_{NAC} = A_{AC}(P_{NAC}-P_{AC})^{\eta_{AC}} + B(P_{NAC}-P_{AC}) \qquad [2c]$$

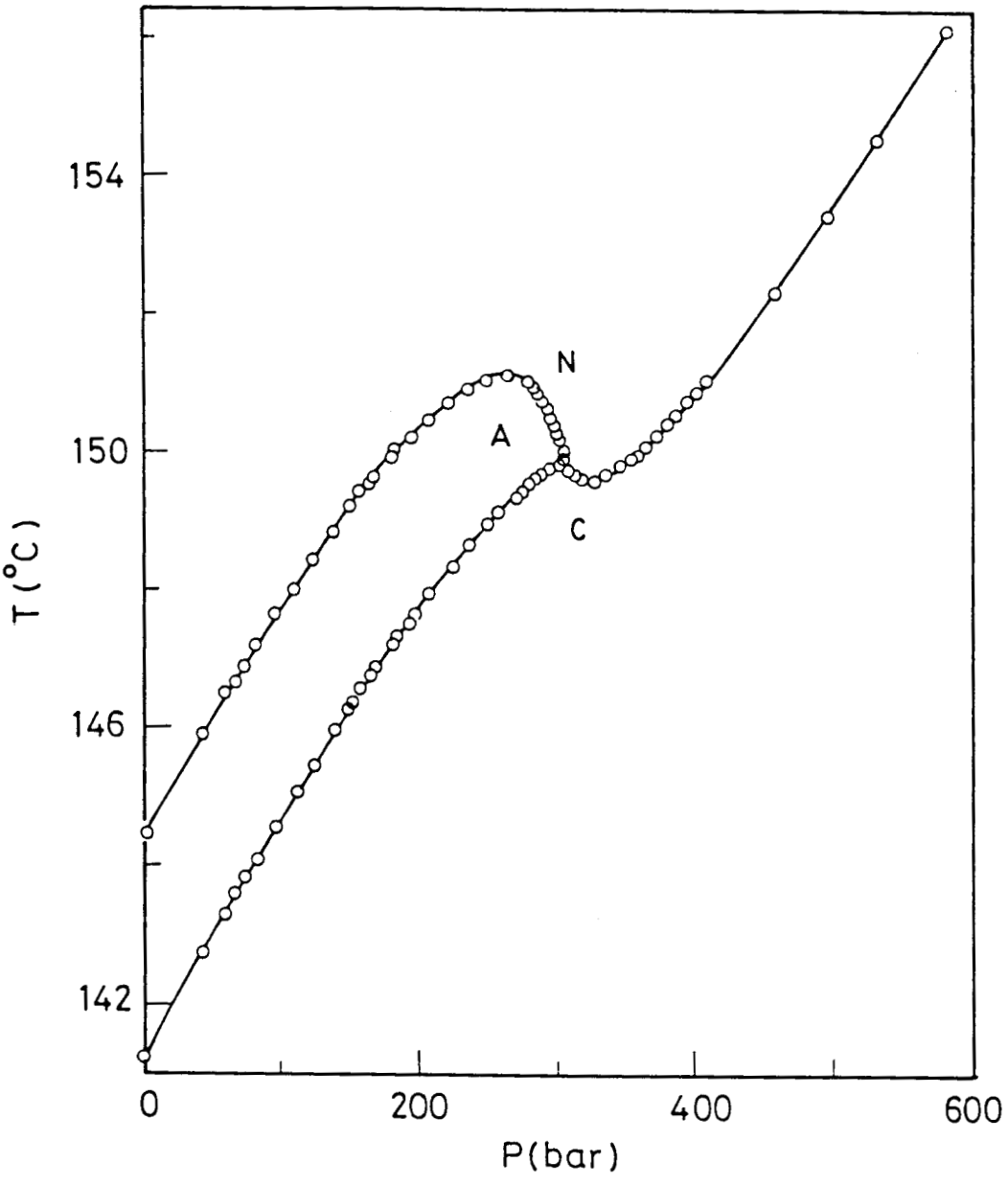

Figure 3.5

Pressure-temperature (P-T) diagram of 7APCBB showing NA, AC and NC transitions up to 600 bar. Solid lines are guides to the eye (ref. 14).

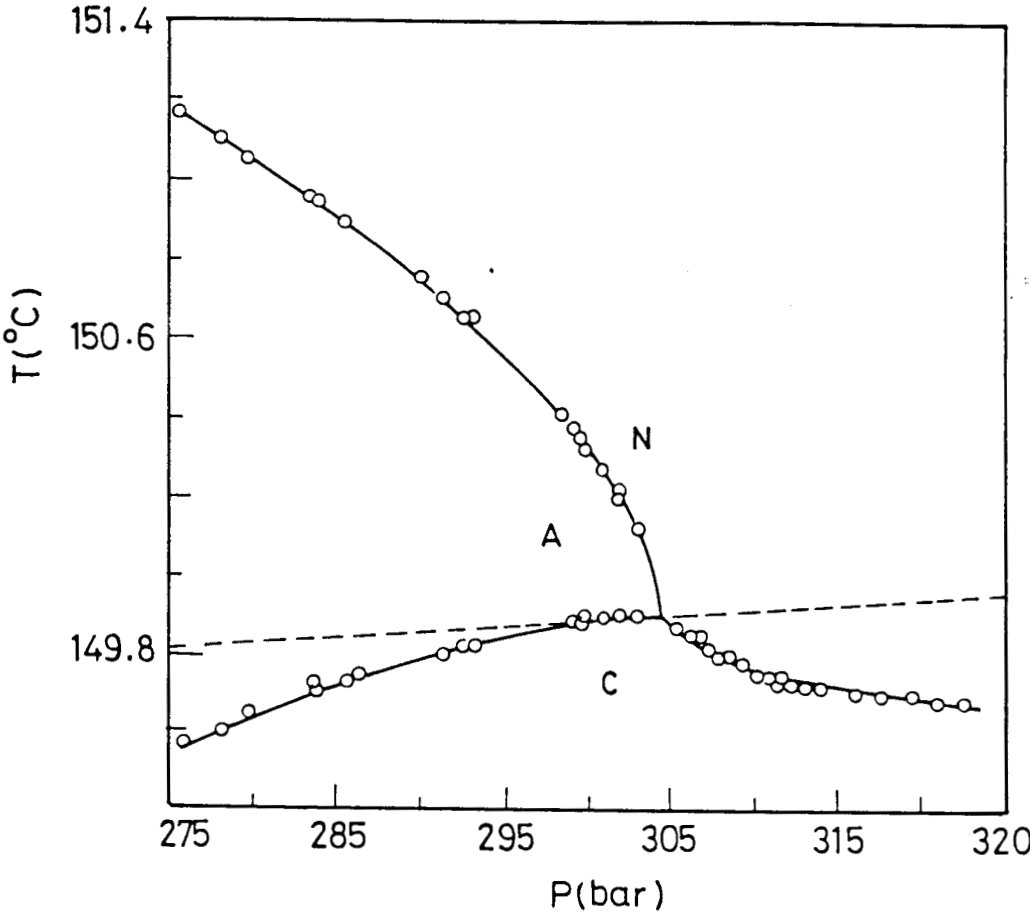

Figure 3.6

High resolution P-T diagram in the vicinity of the NAC multi-critical point in 7APCBB. The solid lines are computer fits of our data (see table 3.2) with equations 2a-2c representing the NA, NC and AC phase boundaries respectively. The dashed line represents the line corresponding to the best-fit B term (ref. 14).

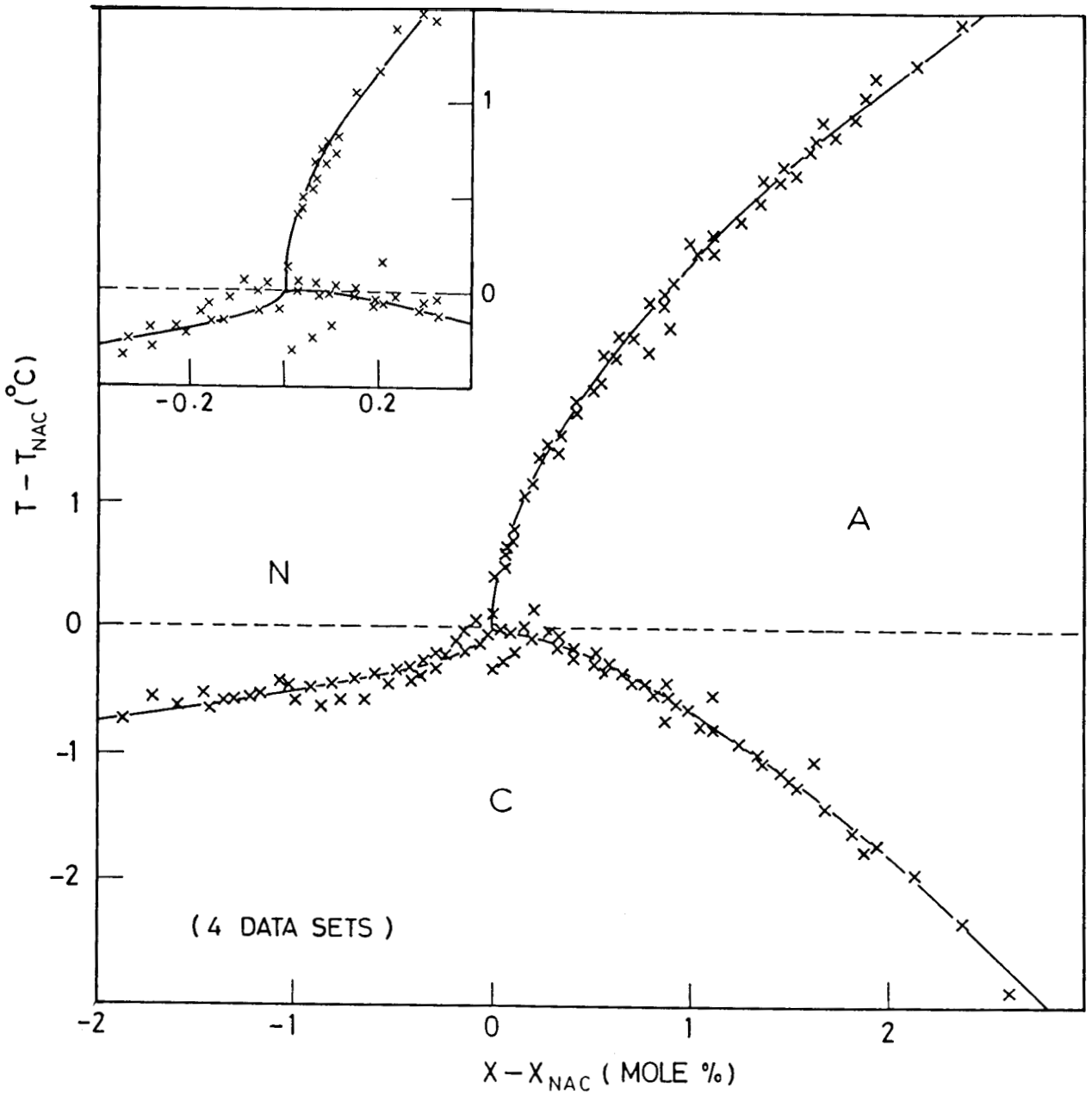

Figure 3.7

The universal temperature-concentration plot of Johnson (see ref. 15) showing the data for four binary liquid crystal systems separately in Fig. 3.4.

The computations were carried out with the universal constraint $\eta_{NA} = \eta_{NC}$ but η was left as a free parameter. The results of the computations carried out using the high resolution P-T data reported in Fig.3.6 are given in Table 3.2. It is clear by comparing with the table of Brisbin et al. (Table 3.1) that the exponents η evaluated in both the cases are same although the amplitude ratio A_{NA}/A_{NC} comes out to be different, -3.02t0.2 in this case, as compared to -5.96 ± 1.3 of Brisbin et al. The remarkable fact that the η values obtained by Shashidhar et al. from the P-T data of a single component system agree exactly with those evaluated from the T- X data of four binary mixtures of Brisbin et al is a strong evidence to support the idea that NAC point exhibits universal behaviour. A noteworthy feature is that the scaling axes are the same as the experimental axes (P and T in the case of Shashidhar et al., T and X in case of Brisbin et al.), rather than a linear combination of these variables. The simplicity of these results may perhaps be associated with the absence of coupling to density and concentration fluctuations.

3.1.2 Reentrant Nematic-Smectic C-Smectic A Multicritical Point (RN-C-A)

Shashidhar et al. in their efforts to look for a NAC point in single component system observed a new kind of multicritical point.[16,17] Pressure studies were carried out by them on 4(4-n-decyloxybenzoyloxy)benzylidene-4'-cyanoaniline[18] which exhibits the follow-

TABLE 32

Best-fit parameters and values of χ^2 for individual fits of high-resolution data for the NA, NC and AC phase boundaries (of 7APCBB) with equations (2a)-(2c) respectively (of ref. 14) (See text for detailed discussions) (Ref. 14)

B	0.003 ± 0.001
T_{NAC}	149.9 ± 0.02°C
P_{NAC}	304.5 ± 0.1 bar
$\eta_{NA} - \eta_{NC}$	0.575 ± 0.02
η_{AC}	1.523 ± 0.02
A_{NA}	0.1731 ± 0.002
A_{NC}	-0.0574 ± 0.0030
A_{AC}	-0.0025 ± 0.0004
χ^2_{NA}	1.056
χ^2_{NC}	0.969
χ^2_{AC}	0.91 1

ing sequence of transitions,

Isotropic → Nematic → Smectic A → Smectic C

Crystal ←— Reentrant nematic J

These studies led to the first observation of the reentrant nematic-smectic C-smectic A multicritical point. The topology of the diagram near the multicritical point was determined with high precision.[19] The global phase diagram is shown in Fig.3.8 while the data close to the RN-C-A point are shown in Fig.3.9. The striking feature of this phase diagram exhibiting RN-C-A point was that the singularities were conspicuously absent on the NC and A-RN boundaries which were in fact collinear at the RN-C-A point. At about the same time binary phase diagrams exhibiting RN-C-A point in temperature-concentration plane were reported both by the Bordeaux group[20] and the Halle group.[21] Although none of these were high resolution studies, it appeared that the singularities were absent in some cases (Fig.3.10) while in some other cases they were present (Fig.3.11) though to a less pronounced extent compared to NAC system. This was an extremely puzzling result. The symmetries of the different phases which constitute the RN-C-A point and the NAC point being the same it is to be expected[22] that both of them should belong to the same universality class and hence should exhibit the same type of universal behaviour with regard to the topology of the phase boundaries. This should be true even though the temperature sequence of transitions

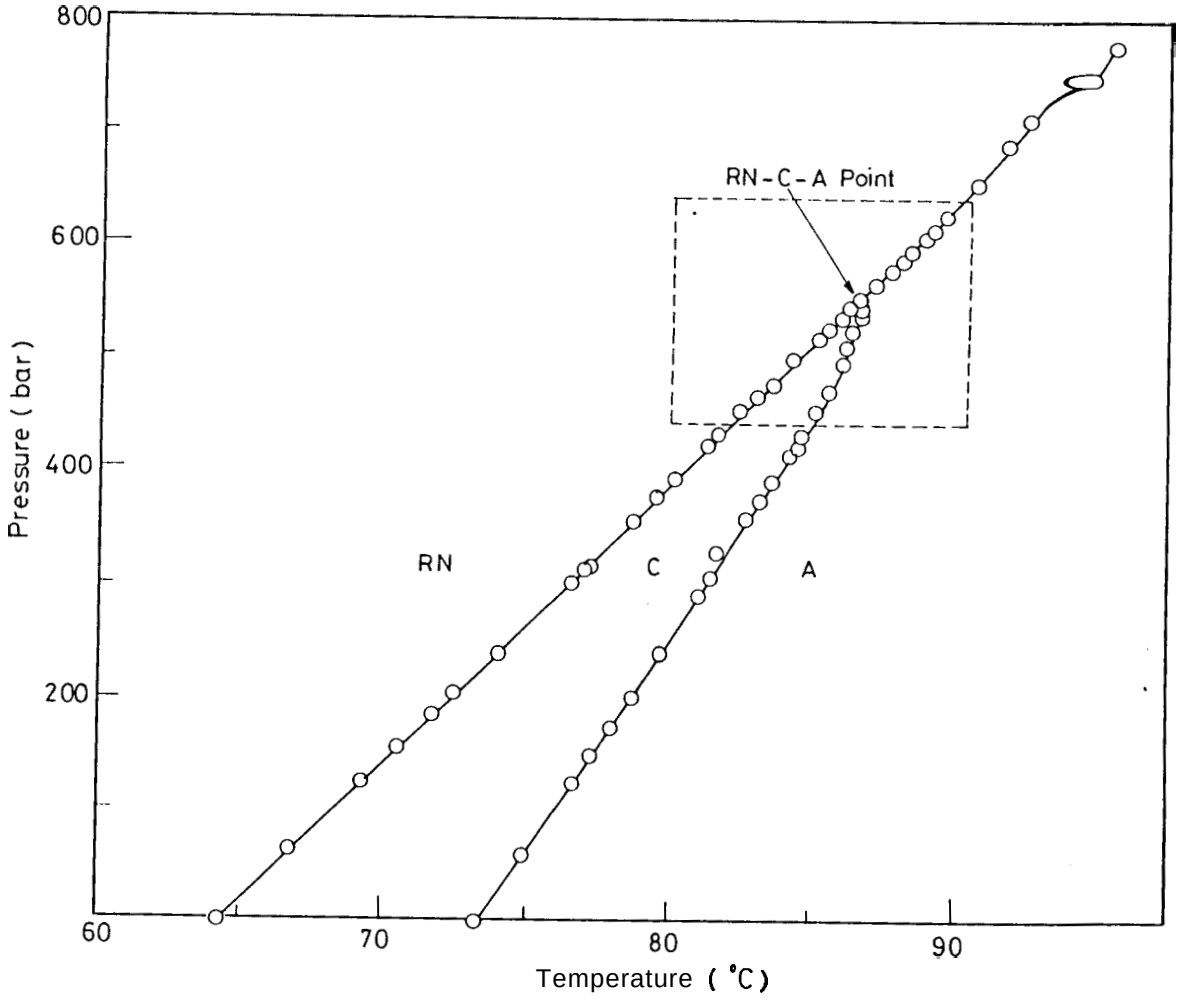

Figure 3.8

P–T diagram of DOBBCA showing the data for the RN–C–A phases up to 800 bar. The section enclosed in dashed lines is shown in an enlarged scale in Fig. 3.9 (ref. 19).

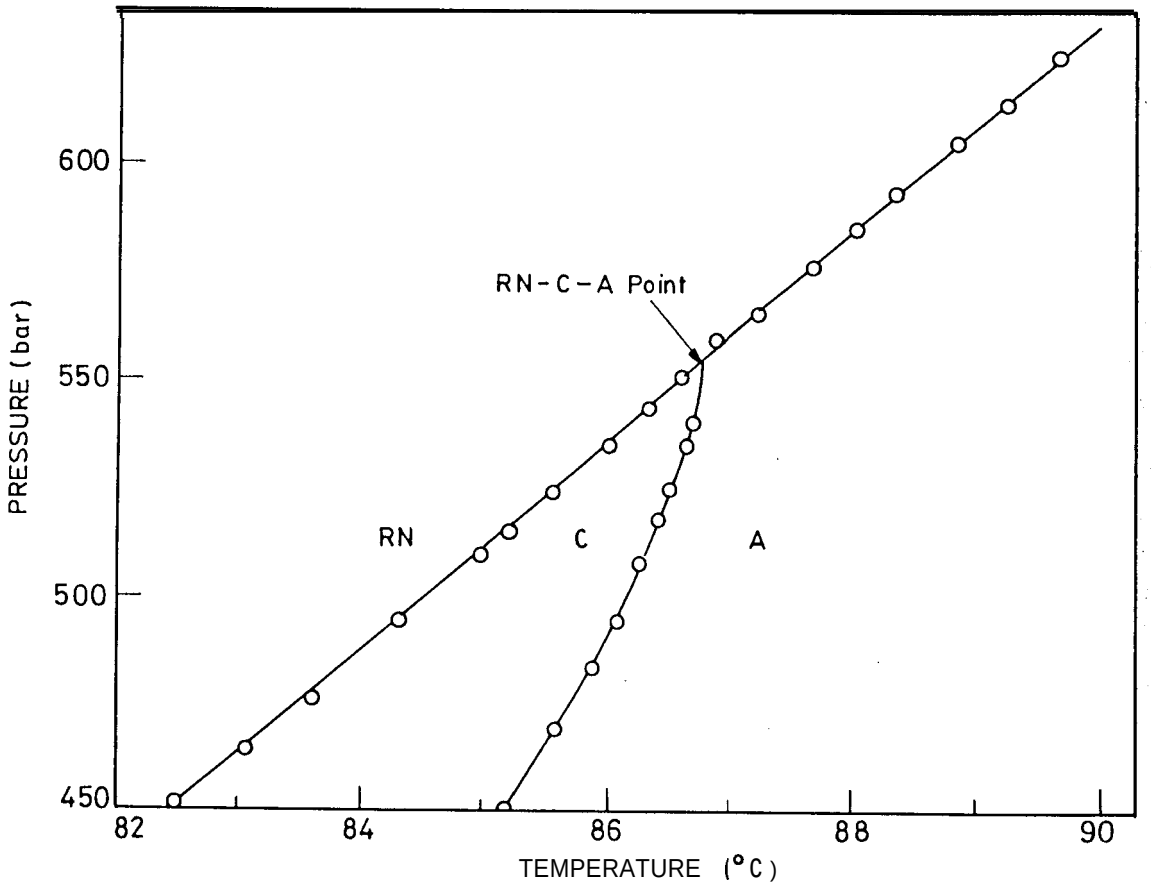

Figure 3.9

Enlarged section of the P-T diagram of DOBBCA in the vicinity of the RN-C-A multicritical point. No singularities are seen on the RN-C or RN-A lines (Ref. 19).

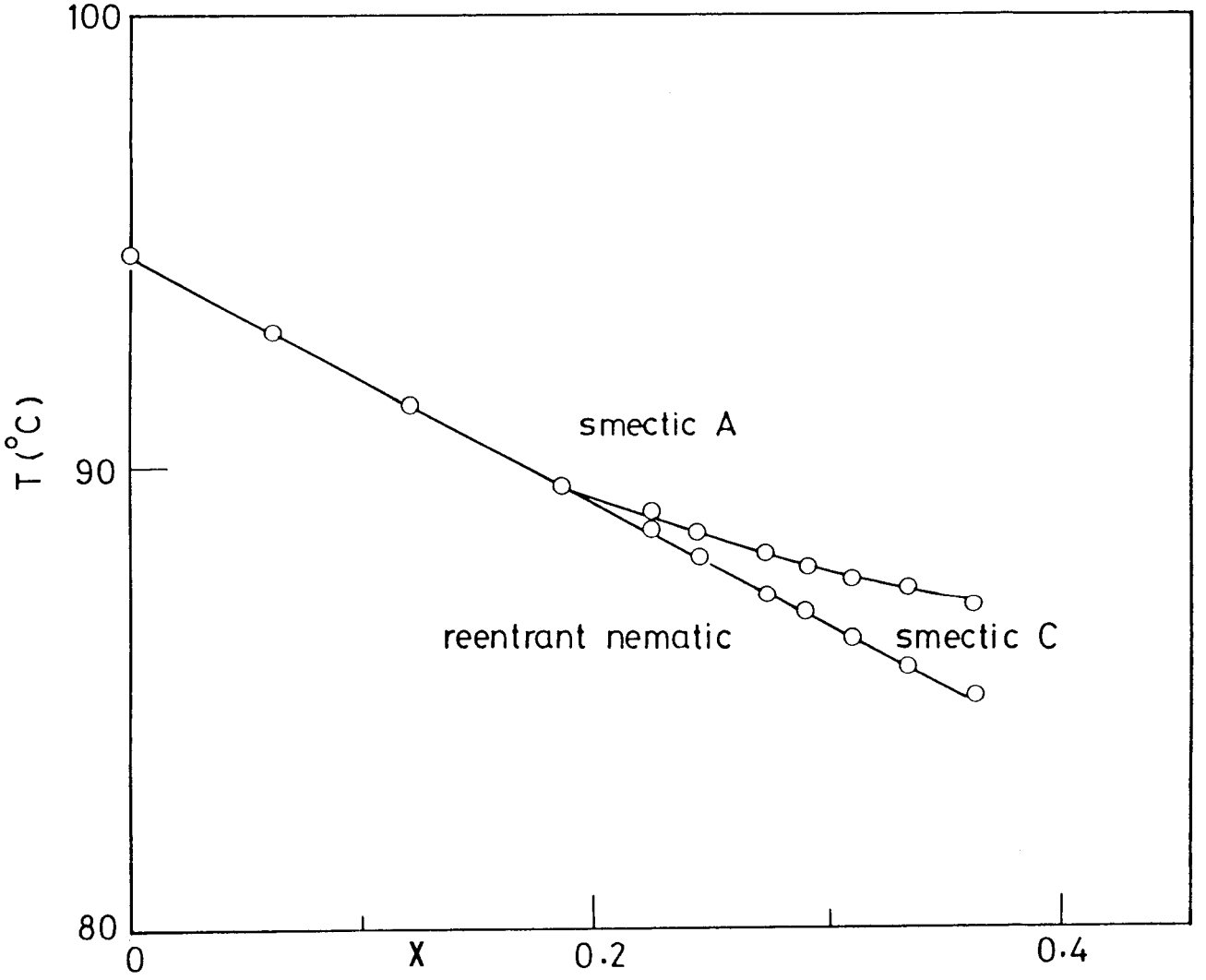

Figure 3.10. Binary isobaric phase diagram of DOBBCA and 4-cyanobenzylidene-4'-(4"-decyloxy benzoyloxy) aniline. X denotes the mol fraction of DOBBCA in the mixture (ref.20

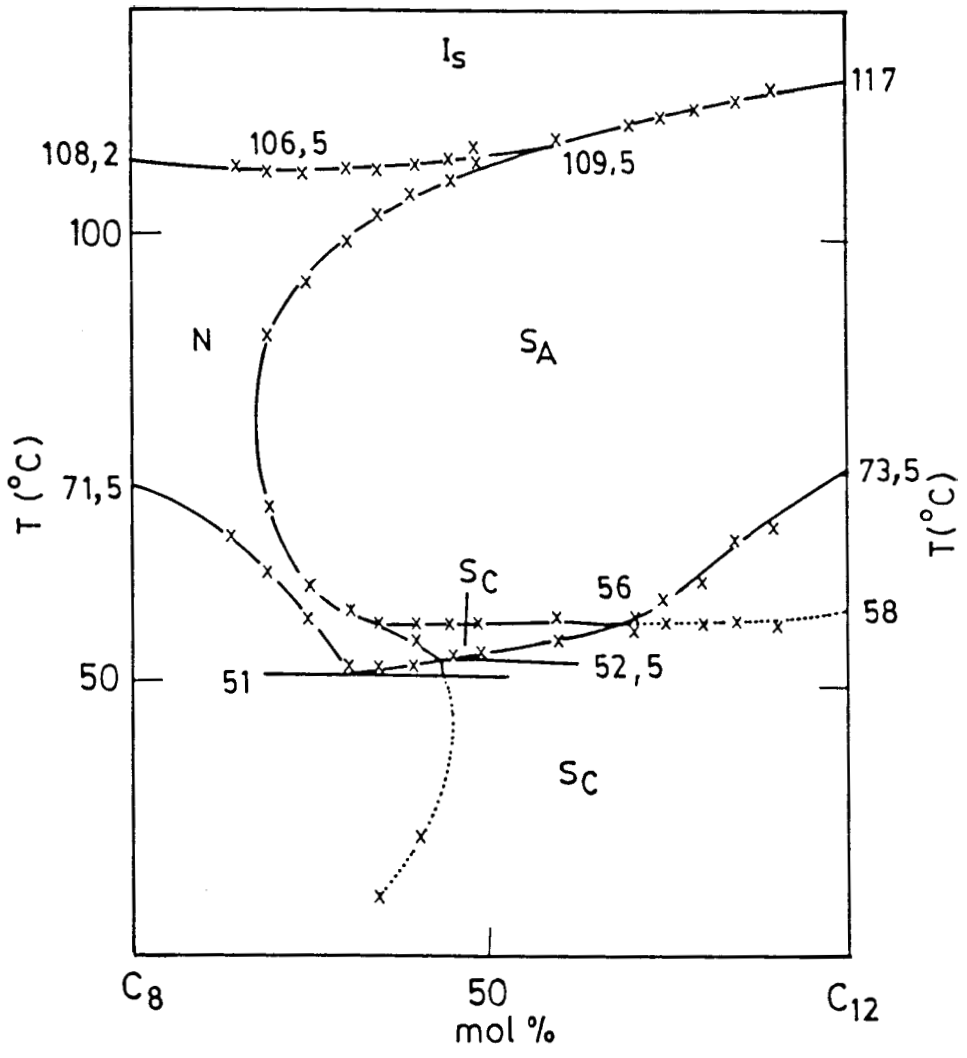

Figure 3.11

Concentration-temperature diagram of 4-(β-cyanoethyl)-phenyl-4-n-dodecyloxy cinnamate + 4-(β-cyano ethyl)-phenyl 4-n-octyloxy cinnamate showing RN-C-A point (ref. 21).

are different in the case of the two multicritical points.

To resolve this problem, high resolution experiments to obtain accurate T-X data near RN-C-A point were undertaken. In order to make sure that the precision in these studies is sufficient to obtain reliable value of η, experiments were initially conducted on a binary system exhibiting NAC point.

3.2 Experimental Technique of Making Binary Mixtures

As remarked earlier, experiments were initially conducted on a binary system exhibiting the NAC point to perfect the technique of achieving very high precisions in the determination of concentration of mixtures and the transition temperatures of the phase transitions. The major problem that was encountered in this regard was the non-availability of sufficient quantities of the material. It is evidently not difficult to achieve a precision of 0.01% or better in concentration when large quantities of material can be weighed. In our case, however, the quantities of the substances available were only of 200-250 mg each and with this limited quantity it was necessary to make at least 25-30 individual concentrations, each with as high an accuracy in concentration as possible. This was achieved in the following way:

a) Weighing.

A Perkin-Elmer (AD II) balance was used for weighing. The balance has an accuracy of 1 microgram. Care was taken to mount

the balance on a massive supporting table so that vibrations did not affect the balance. The constancy in the reading of the balance for any given weighing depends on a number of factors like the constancy of room-temperature, the humidity of the atmosphere and the time for which the balance is allowed to equilibriate. The effect of these factors was minimised by accurate control of the ambient temperature and humidity and waiting for long periods (generally 2 to 3 hours) before any reading was taken for each weighing. Despite these precautions it was observed that the balance reading was never truly constant, and there was a very small but perceptable drift. This problem was overcome by quantitatively analysing the amount of drift as a function of time. Typically, after a waiting period of about 2 hrs, the drift was 1 microgram per hour. It became even less after waiting for still longer intervals. The mapping of drift as a function of time permitted to get the exact weight when extrapolated to zero drift. In this manner, it was possible to obtain a weighing accuracy of ±1 microgram even when the total weight of the mixture was only about 8-10 mg. The samples were weighed on a very thin glass coverslip. Care was taken to see that the samples added on to the coverslip are at the centre of the coverslip and form a heap. Even a speck of the sample was not allowed to spill outside the heap while the samples were being added.

b) Method of preparation of mixtures and determination of transition temperature.

For every concentration a new mixture was made in the manner described below. After weighing on a coverslip the requisite amounts of constituent materials, the coverslip along with the sample was transferred on to a temperature controlled oven. The two materials were mixed thoroughly at a temperature well above their melting temperatures. A drop of the molten mixture was transferred to a coverslide for determination of the transition temperatures. The mixtures used in this way were stored in an evacuated atmosphere for any future work. The homogeneity in mixing was ascertained by the sharpness of the transitions as seen by a polarising microscope. Generally, a concentration gradient due to bad mixing manifests as a large width in the transition temperature when viewed optically. In such a case the mixture was discarded and a fresh mixture was made. All the transition temperatures were determined using a polarizing microscope (Leitz, Orthoplan) equipped with a video recording system as well as still photographic attachment. This was used in conjunction with a Mettler hot stage (FP52) and temperature controller (FP800). The rough transition temperature was determined by adopting a heating or cooling rate of 1°C/min. All global phase diagrams shown in this thesis were studied with this rate (1°C/min). However for high-resolution work a rate of 0.2°C/min, the minimum rate permissible with this system, was always used. The temperature reading accuracy

was O.I°C. However, we were able to achieve an order of magnitude higher accuracy by the following procedure. Using a digital timer synchronously with the Mettler system, it was possible to interpolate accurately the temperatures of the stage to an accuracy of 10 mK. Therefore, in our high resolution studies, the determination of transition temperature was ±10 mK while the accuracy in the determination of concentration was ±0.01%.

3.3 EXPERIMENTAL STUDIES ON NAC SYSTEM

The substances investigated for the study of the NAC point are 4,4'-di-n-heptyloxyazoxybenzene (HOAB) and 4-n-octyloxyphenyl-4'-cyanobenzoate (8OPCB). The molecular structures and the transition temperaturtes of these compounds are shown in Fig.3.12. One of the compounds, HOAB exhibits smectic C and nematic phases while the other (8OPCB) exhibits nematic, smectic A and a highly metastable smectic C phase. The C phase is just formed and within about 0.2°C the crystallization takes over, when the transitions are seen optically.

On mixing these compounds and studying the transition temperatures for a few mixtures with larger concentration gap, a phase diagram shown in Fig.3.13 is obtained. The nematic phase gets bounded on both sides due to increased thermal stability of smectic A phase in the intermediate range of concentrations. The NAC point is located at 97.6°C and a concentration of 12.2 mol % of HOAB in the mixture. Even from the global phase diagram (Fig. 3.13) strong singularities

HOAB

4 , 4' — di — n — heptyloxy — azoxybenzene

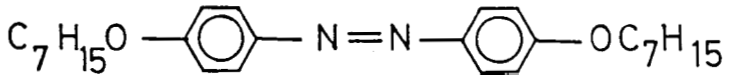

Sequence of transitions

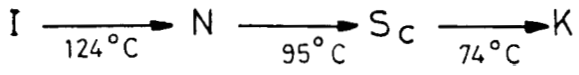

80PCB

4 — n — octyloxyphenyl-4' — cyanobenzoate

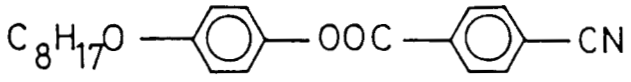

Sequence of transittons

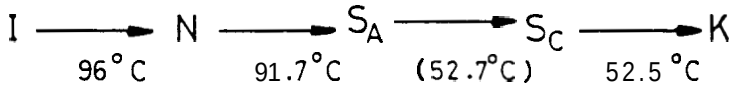

( ) denotes that the transition is monotropic

Figure 3.12

Chemical structure and sequence of transitions.

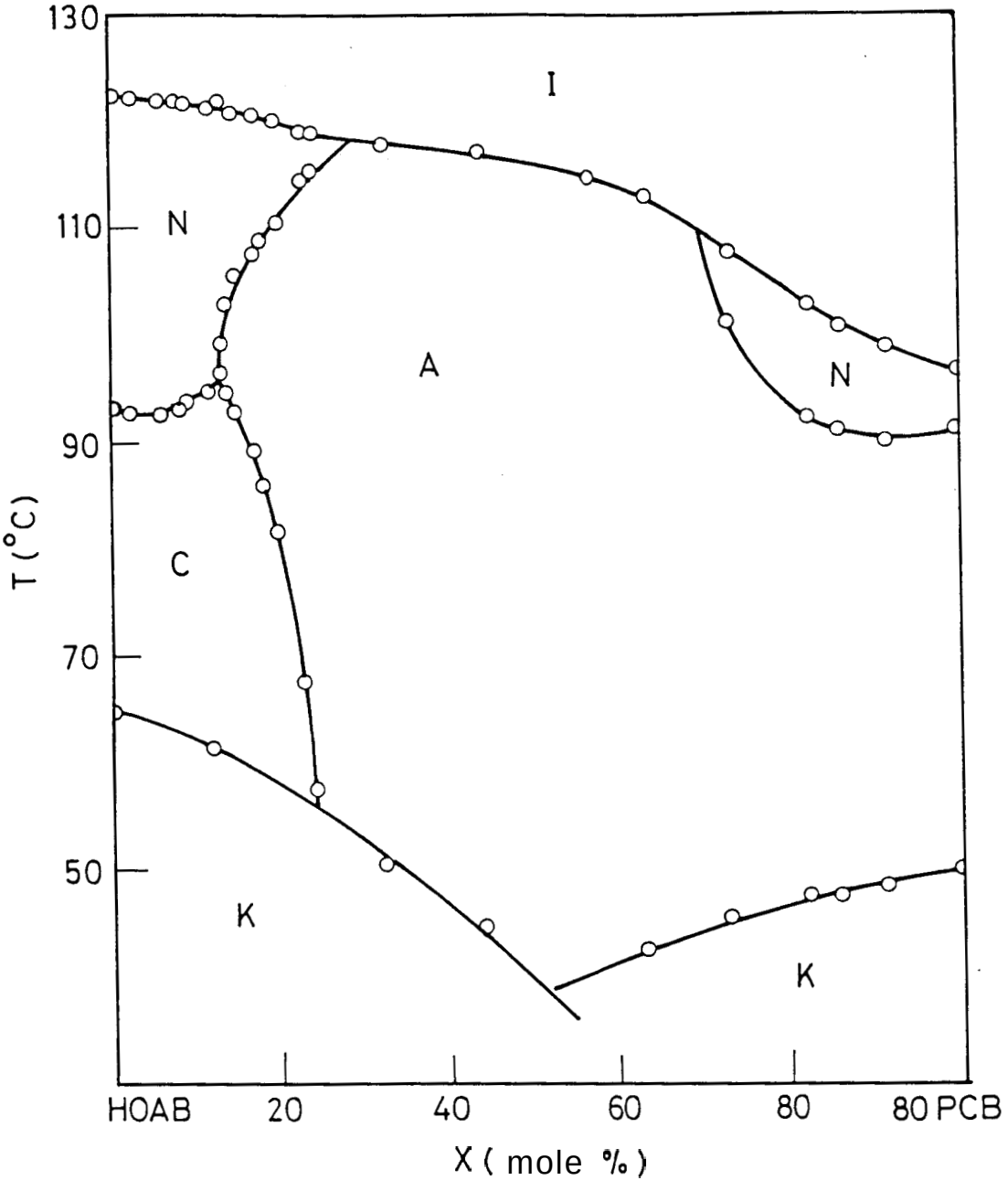

Figure 3.13

Temperature-concentration diagram of HOAB/8OPCB showing NAC point. Solid lines through the data are guides to the eye. X is mol % of 8OPCB in the mixture.

on the NA, AC and NC boundaries in the vicinity of the NAC point are visible.The smectic A-smectic C boundry in particular, has a very steep curvature. The high-resolution data collected in the immediate vicinity of the NAC point are shown in Fig.3.14. It is clear that our high resolution temperature-concentration diagram is strikingly similar to the universal diagram of Johnson et al. (Fig. 3.7). We shall now examine the phase boundaries quantitatively in the proximity of the NAC point.

Using the expressions [1a] and [1b] and with universal constraint $\eta_{AN} = \eta_{NC}$, computations were carried out keeping η, T_{NAC} and X_{NAC} as free parameters. The results of our computations carried out with high resolution data represented in Fig.3.14 are given in table 3.3. It is immediately clear that the exponent η obtained for HOAB-8OPCB system is identical to the universal exponents of Brisbin et al. (Table 3.1) in the (T-X) plane and Shashidhar et al. (Table 3.2) in the (P-T) plane. The goodness of the fit is evident from the Fig. 3.14 where the solid lines denote the computer fits of the data with η, A and B values given in the table 3.3. Thus we have ascertained that we can achieve in our temperature-concentration experiments very high precisions in the determinations of concentration and transition temperature which are required for an accurate determination of η and hence our probing the universal behaviour near the multicritical point. With this experience we set out to investigate the reentrant

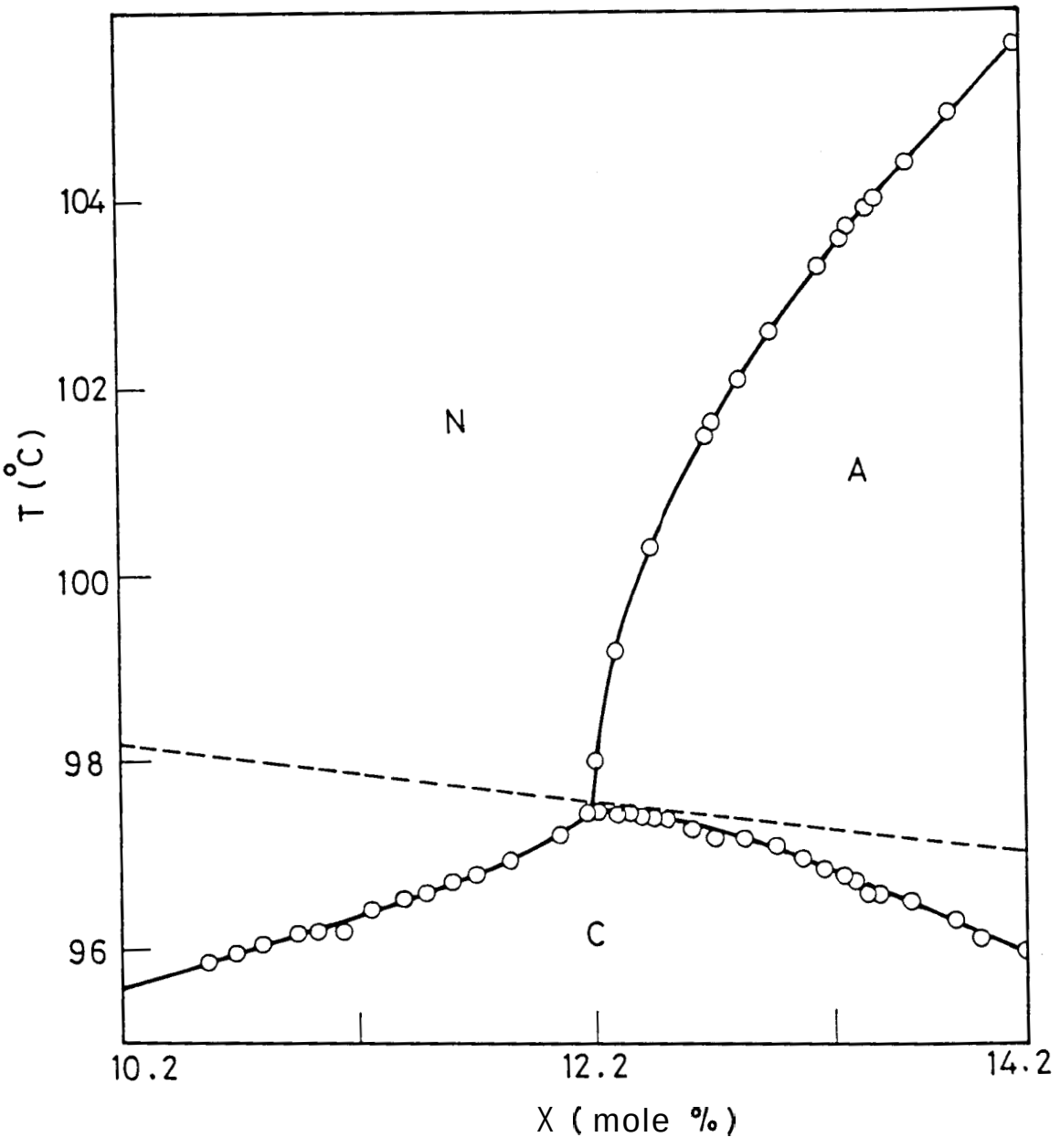

Figure 3.14

High resolution T–X diagram of HOAB/8OPCB in the vicinity of NAC point. X is mole % of 8OPCB in the mixtures. Solid lines are computer fits of our data (see table 3.3) with equations 1a–1b representing NA, AC and NC boundaries respectively. The dashed line represents the line corresponding to the best–fit B term.

TABLE 3.3

Best-fit parameters and values of χ^2 for individual fits of high-resolution data for the NA, NC and AC phase boundaries (of HOAB-8OPCB binary system) with equations (1a) and (1b) respectively.

B	-0.3 ± 0.02
T_{NAC}	97.6°C
X_{NAC}	12.2 mol %
$\eta_{NA} = \eta_{NC}$	0.574 ± 0.02
η_{AC}	1.535 ± 0.003
A_{NA}	6.185 ± 0.015
A_{NC}	-0.940 ± 0.002
A_{AC}	-0.44 ± 0.01
χ^2_{NC}	1.021
χ^2_{NA}	1.073
χ^2_{AC}	0.998

nematic-smectic C-smectic A point.

3.4. STUDIES ON RN-C-A SYSTEM

Before proceeding to present our results on the RN-C-A point, let us examine some of the temperature-concentration and pressure-temperature diagrams reported so far which exhibit the RN-C-A point. Fig. 3.15 shows temperature-concentration diagram due to Sigaud et al.[20] and Fig. 3.16a shows pressure-temperature diagram of DOBBCA due to Shashidhar et al.[16] It is interesting that the material DOBBCA for which P-T diagram is studied (Fig. 3.16b structure and transition) is also one of the components of T-X diagram shown in Fig.3.15. The absence of singularities near RN-C-A point is clear from both the diagrams (Fig. 3.1 5 and Fig. 3.16a). It is to be pointed out that the RN-C-A point is located very far in temperature scale from N-I transition (– 180°C) in P-T plane and (~ 170°C) in the T-X diagram of Sigaud et al. Due to this large temperature difference between $T_{C\text{-}RN}$ (near RN-C-A) and $T_{N\text{-}I}$, it is conceivable that the Brazovskii fluctuations which are believed to induce the nematic-smectic C transition first order might be extremely weak near RN-C-A point. We shall enumerate this point in some detail in the following.

It is possible to describe the smectic C phase with a complex order parameter whose magnitude gives the tilt angle between the director and the density wave, and, whose phase corresponds to azimuthal rotation of the molecules about a direction which is normal

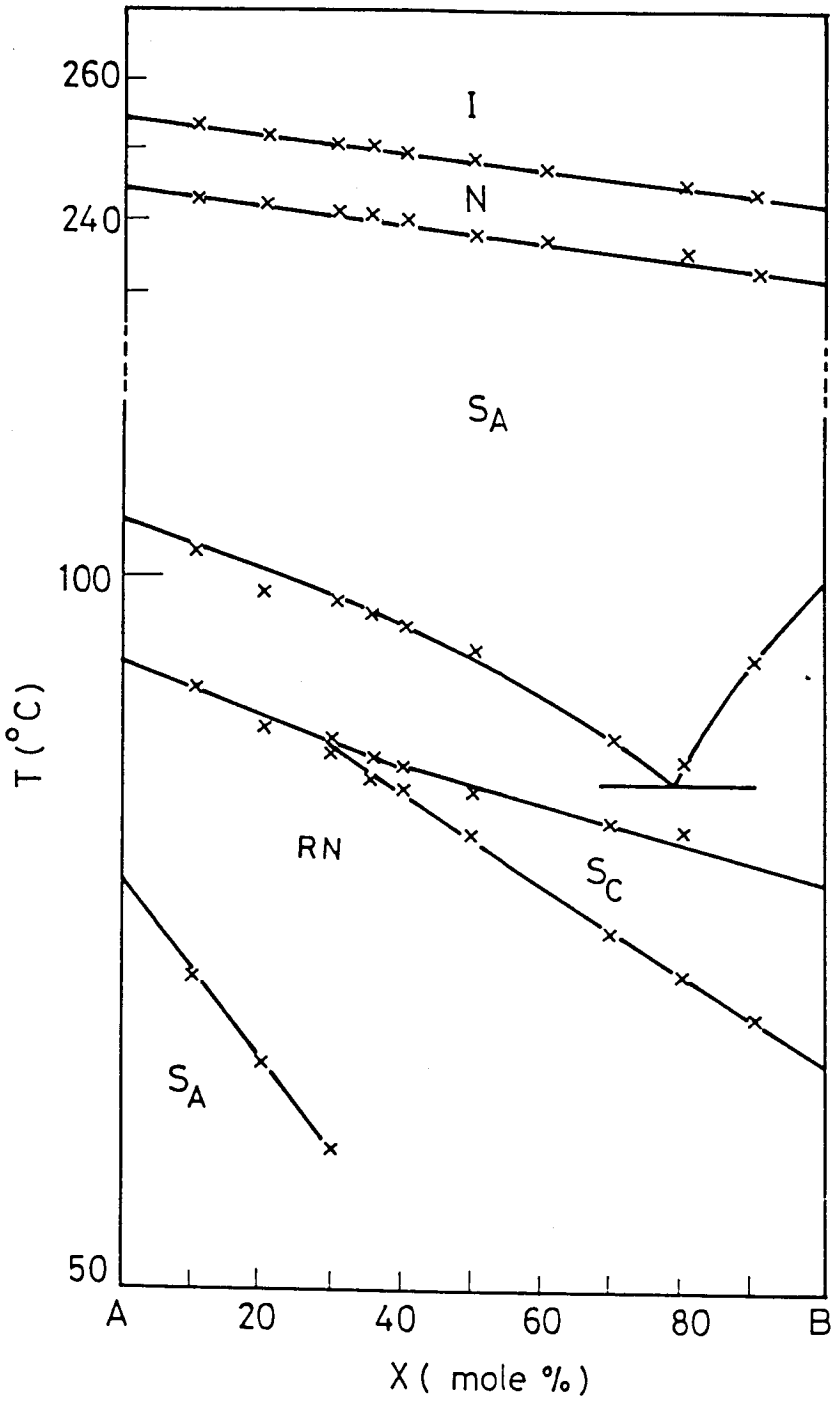

Figure 3.15

Binary isobaric diagram (1 atmospher) of 9OBCAB (A) and DOBBCA (B) exhibiting $N_{re}AC$ point. X is mol % of B in the mixture (ref. 20).

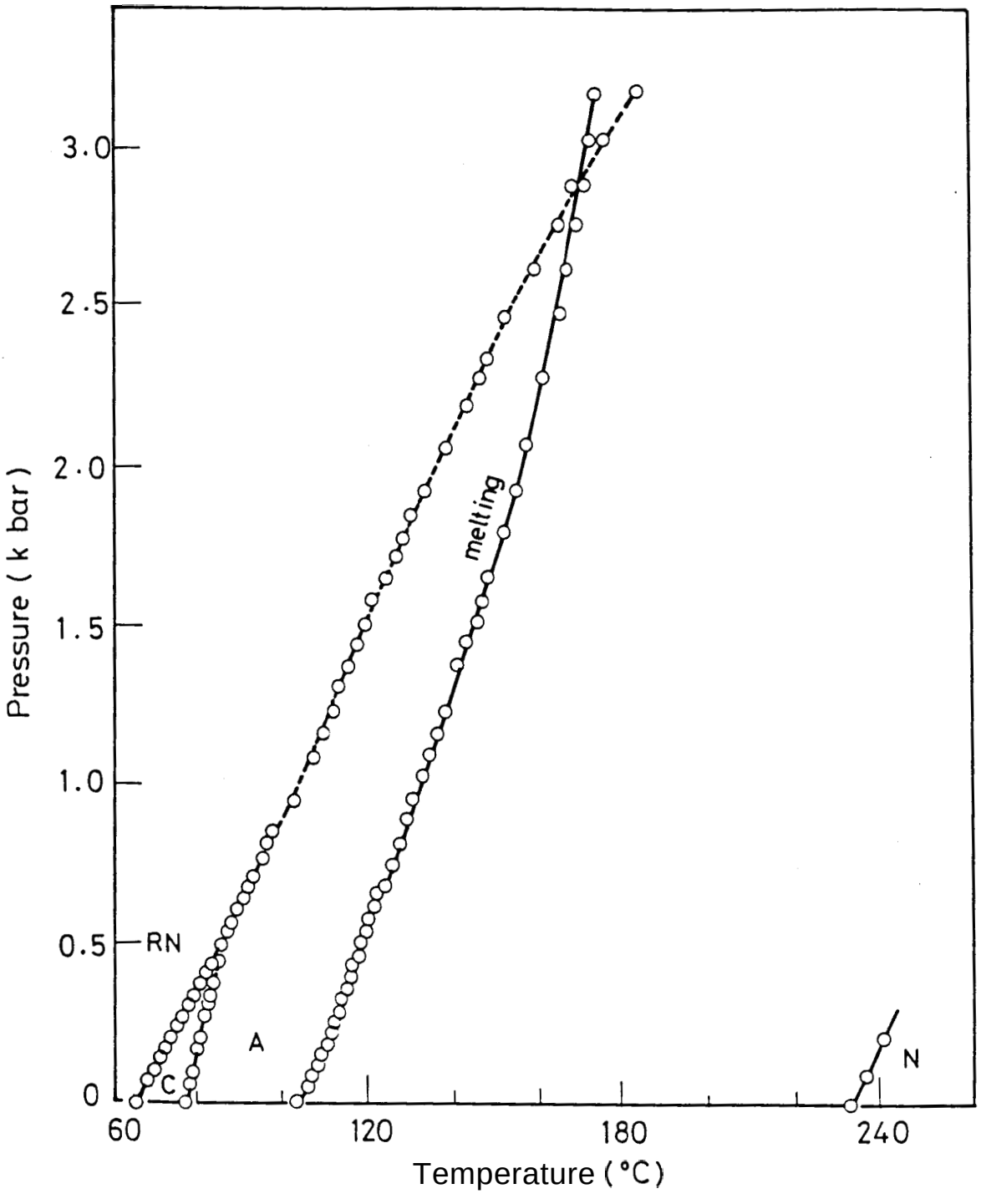

Figure 3.16a

P–T diagram sf DOBBCA by Shashidhar et al. (ref. 16)

Chemical formula of DOBBCA

4 (4 –n– decyloxy benzoyloxy) benzylidene – 4^{I} cyanoaniline

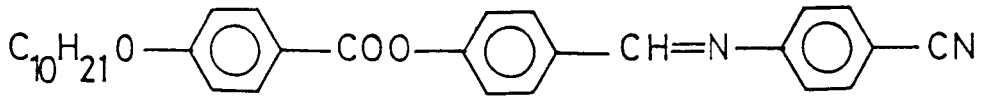

Sequence of transitions

$$I \xrightarrow{242^{\circ}C} N \xrightarrow{232.1^{\circ}C} S_A \xrightarrow{(79.1^{\circ}C)} S_C \xrightarrow{(66.2^{\circ}C)} R_N \xrightarrow{58.7^{\circ}C} K$$

( ) denotes that the transitions are monotropic

Figure 3.16(b)

to the layers. The symmetry of this order parameter does permit a second order phase transition between smectic C and nematic phases. However nematic-smectic C transition is experimentally observed to be always first order. The reason for this is quite interesting. It was shown by Brazovskii[23] that if a density wave is established with infinite number of possible characteristic wavevectors in a material, such a system will always exhibit only a first order phase transition due to the effect of fluctuations. It was pointed out by Swift[24] that the nematic-smectic C transition belongs to Brazovskii's class. Thus the nematic-smectic C transition is expected to be always first order even though mean field theories which omit the effect of such fluctuations predict second order behaviour.

As remarked earlier the location of the nematic-smectic C transition (near RN-C-A) far way in temperature from the nematic-isotropic transition creates an interesting situation. Under such a condition the Brazovskii fluctuations can be very weak and the nematic-smectic C transition can become, in principle, second order. It would also have the effect that the bare correlation length would become very large so that the critical region would be too small to be observed experimentally. This situation is similar to the mechanism which causes a mean field-like behaviour in spin-reorientation transitions in magnetic systems.[25]

The question therefore arises whether the critical region in

the vicinity of RN-C-A point can be increased by tuning the Brazovskii fluctuations, i.e., by bringing the nematic-isotropic transition closer to RN-C-A point. With this in view we undertook the study of temperature-concentration diagrams of several binary systems with different structures and hence different transition temperatures. Results on two of these systems are given in the following.

The systems studied were binary mixtures of 4-cyanoethylphenyl-4'-octyloxy cinnamate (CEPOOC) and 4'-octyloxyphenyl-4-cyanobenzoate (8OPCB) and 4-cyanoeth ylphenyl-4'-decylox y cinnamate (CEPDOC) and CEPOOC. The chemical formulae of the different materials are shown in Figures 3.17 and 3.12 and the transition temperatures are listed in table 3.4. The complete binary concentration-temperature diagram for mixtures of CEPOOC and 8OPCB is shown in Fig.3.18. The compound CEPOOC has only nematic phase while the other component 8OPCB has nematic, smectic A and smectic C phases. But interestingly, when they are mixed, because both of them possess strongly polar end groups, the smectic A-nematic boundary curls pronouncedly with increasing concentration of CEPOOC leading to the exhibition of reentrant nematic phase over quite a large range of concentration. The smectic A-smectic C boundary drops very steeply with even a slight addition of CEPOOC. However this boundary curls backwards as the RN-C-A point is approached. The RN-C-A point is seen at 39.85°C and 45.66 mol % concentration. It is clear that all the three

Chemical structures of CEPOOC and CEPDOC

CEPOOC

4 – Cyano ethylphenyl – 4′ – octyloxy cinnamate

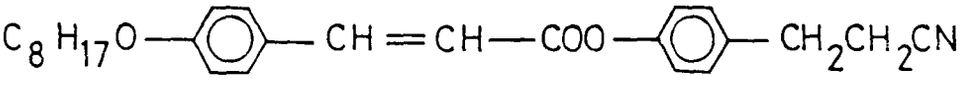

CEPDOC

4 – cyano . ethylphenyl – 4′ – decyloxycinnamate

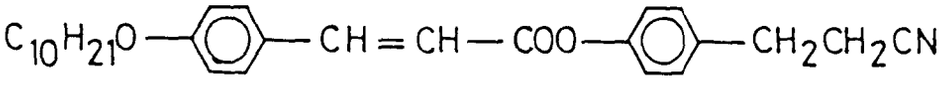

Figure 3.17

TABLE *3.4*

Transition temperatures in °C of CEPOOC and CEPDOC

Substance	K	S_C	A	N	I
CEPOOC	40.3	-	-	108.5	
CEPDOC	72.0	(59.1)	109.0	109.5	

( ) denotes that the transition is monotropic.

For transition temperatures of 8OPCB please see Fig. 3.12.

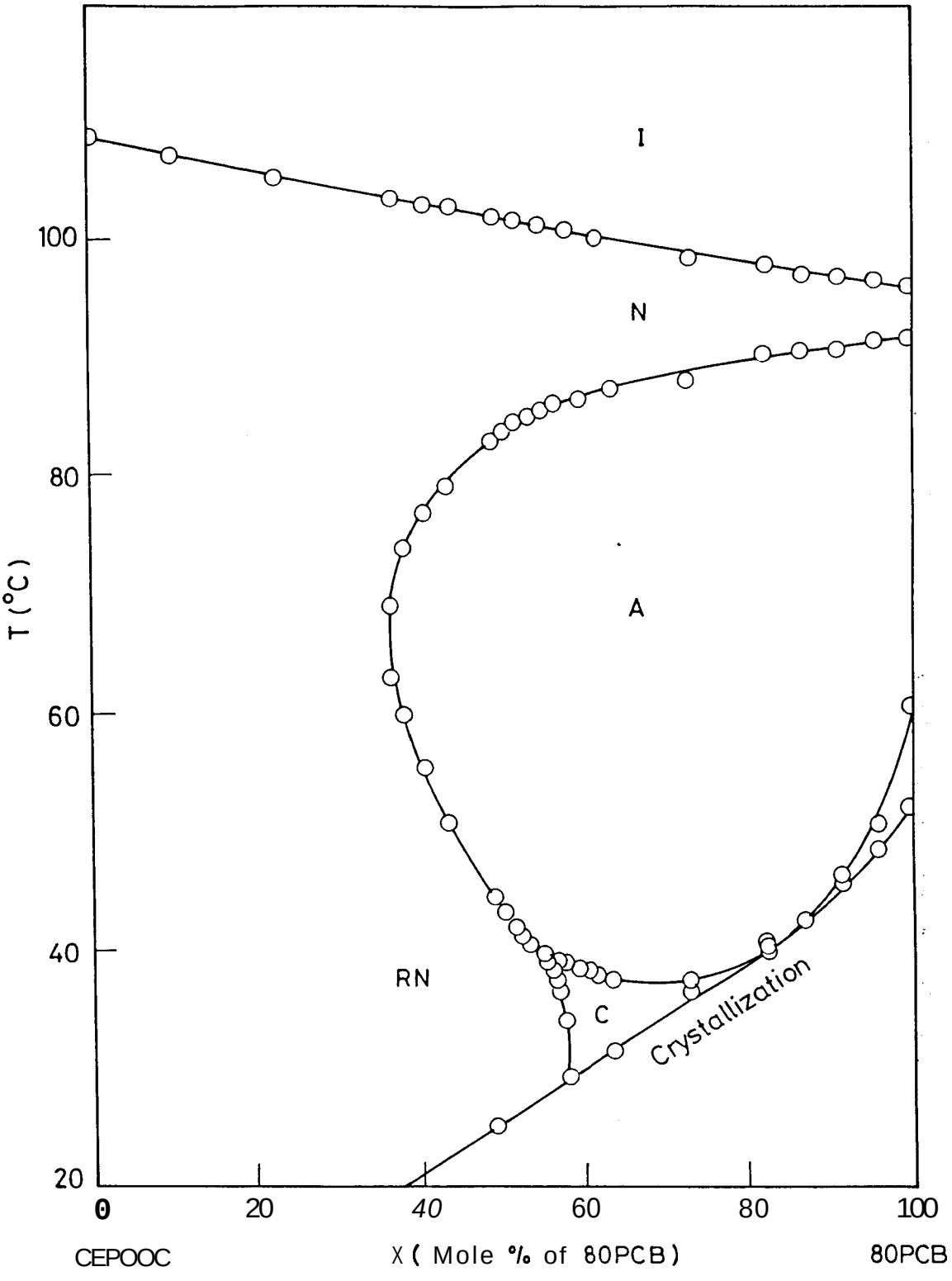

Figure 3.18

Complete temperature-concentration (T-X) diagram for binary mixtures of CEPOOC and 8OPCB. X is mole % of 8OPCB in the mixture. The solid lines are guides to the eye.

phase boundaries, reentrant nematic-smectic A, reentrant nematic-smectic C and smectic C-smectic A have pronounced curvatures in the neighbourhood of RN-C-A point, presumably because of our bringing RN-C-A point close to nematic-isotropic transition temperature - this is about 65°C in this case compared to 170° C in the case of Siguad et al. (Fig. 3.15).

The complete temperature-concentration diagram of the binary mixtures of CEPDOC and CEPOOC is shown in Fig.3.19. Essentially the phase diagram looks the same as that for CEPOOC/8OPCB (Fig. 3.18), the RN-C-A point being observed at 60.84°C and 31.085 mol % concentration. It is now located ~45°C away from the corresponding nematic-isotropic transition in the temperature scale. The feature of this phase diagram (Fig.3.19) is the very high degree of curvature of reentrant nematic-smectic C line on approaching the RN-C-A point. In fact the reentrant nematic-smectic C boundary curls backwards as RN-C-A point is approached leading clearly to a reentrant nematic-reentrant smectic C phase trasition, i.e., in the concentration range of 58-62% of CEPDOC, the sequence of transitions on cooling from the isotropic phase is, isotropic-nematic-smectic A-smectic C-reentrant nematic-reentrant smectic C-crystal. Such instances of reentrant smectic C have been reported before.[21]

<u>High resolution study in the vicinity of RN-C-A point.</u>

The global phase diagrams of CEPOOC/8OPCB (Fig.3.18) and

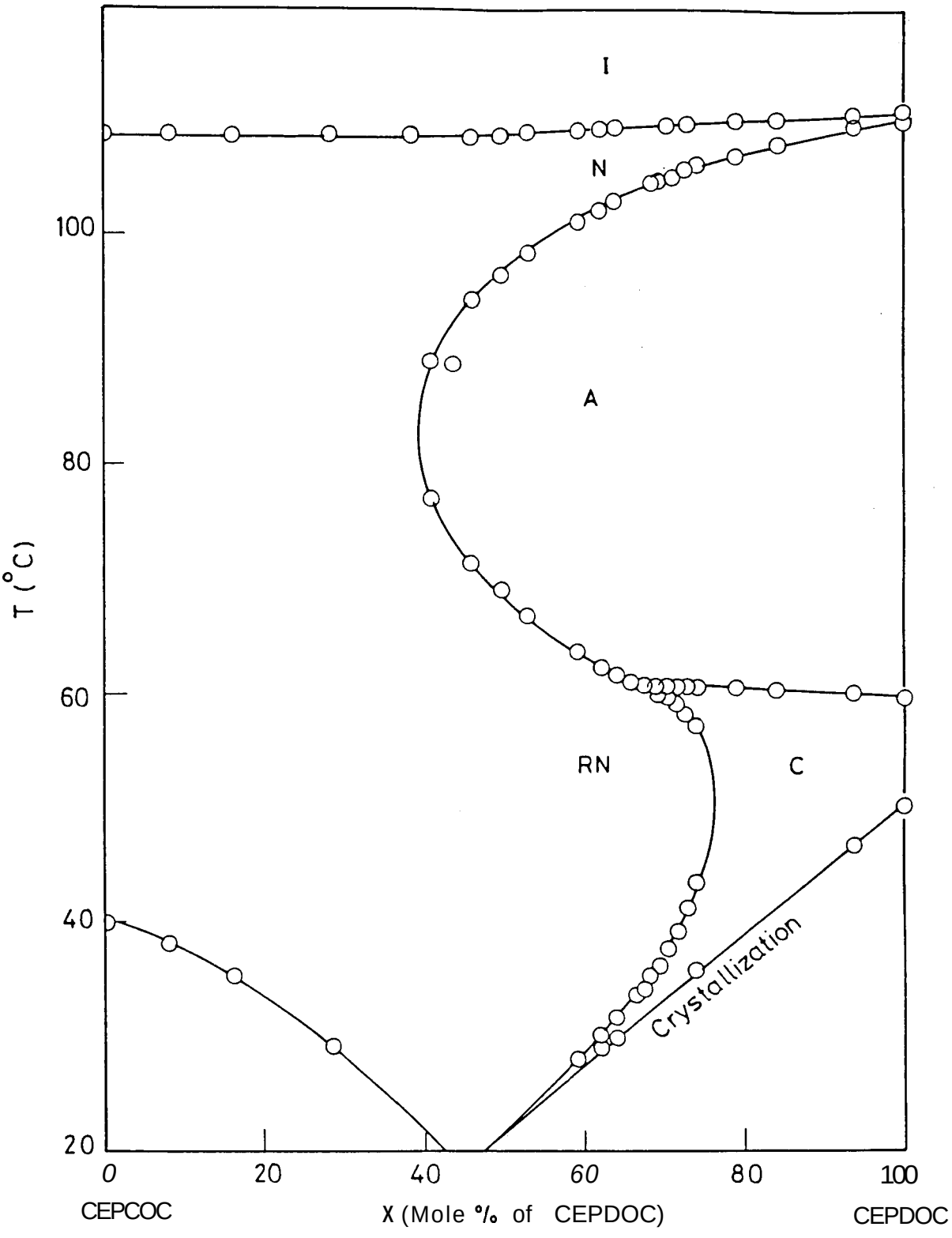

Figure 3.19

Complete T–X diagram for binary mixtures of CEPOOC and CEPDOC. X is mole % of CEPDOC in the mixture. The solid lines serve as guides to the eye.

CEPOOC/CEPDOC (Fig.3.19) were obtained with a precision in concentration −0.1 to 0.2%. Since it is well known that the true critical behaviour can be probed only by accurate data in the immediate vicinity of multicritical point, we carried out an extensive study of the region in the close proximity of the RN-C-A point. As described earlier, for high resolution data collected in this region the accuracy was −3.01 mol %, in concentration and ~±10 mK for transition temperatures. The high resolution data for CEPOOC/8OPCB and CEPOOC/CEPDOC systems are presented in Fig.3.20 and Fig.3.21 respectively. It must be pointed out that typically the size of a circle shown in the global phase diagrams 3.18 and 3.19 constitutes the entire region of the corresponding high resolution diagrams presented in Fig. 3.20 and Fig.3.21. Clearly singularities are seen for all the three phase boundaries. We have plotted the high resolution data with temperature along the x-axis and concentration along the y-axis. The close similarity of Fig.3.20 and 3.21 with universal curves of NAC obtained by Brisbin et al.[12] (Fig.3.4) and Shashidhar et al.[14] (Fig.3.6) is striking. We shall now analyse the singularities near the RN-C-A point quantitatively. It is relevant to recall here that the remarkable feature of the results on NAC multicritical point was that the scaling axes were the same as the experimental axes - P and T in the case of single component system[14] and T and X in the case of binary systems.[12] In our computations on the RN-C-A point we have used essentially the same expressions as those used by Brisbin et al. for the NAC

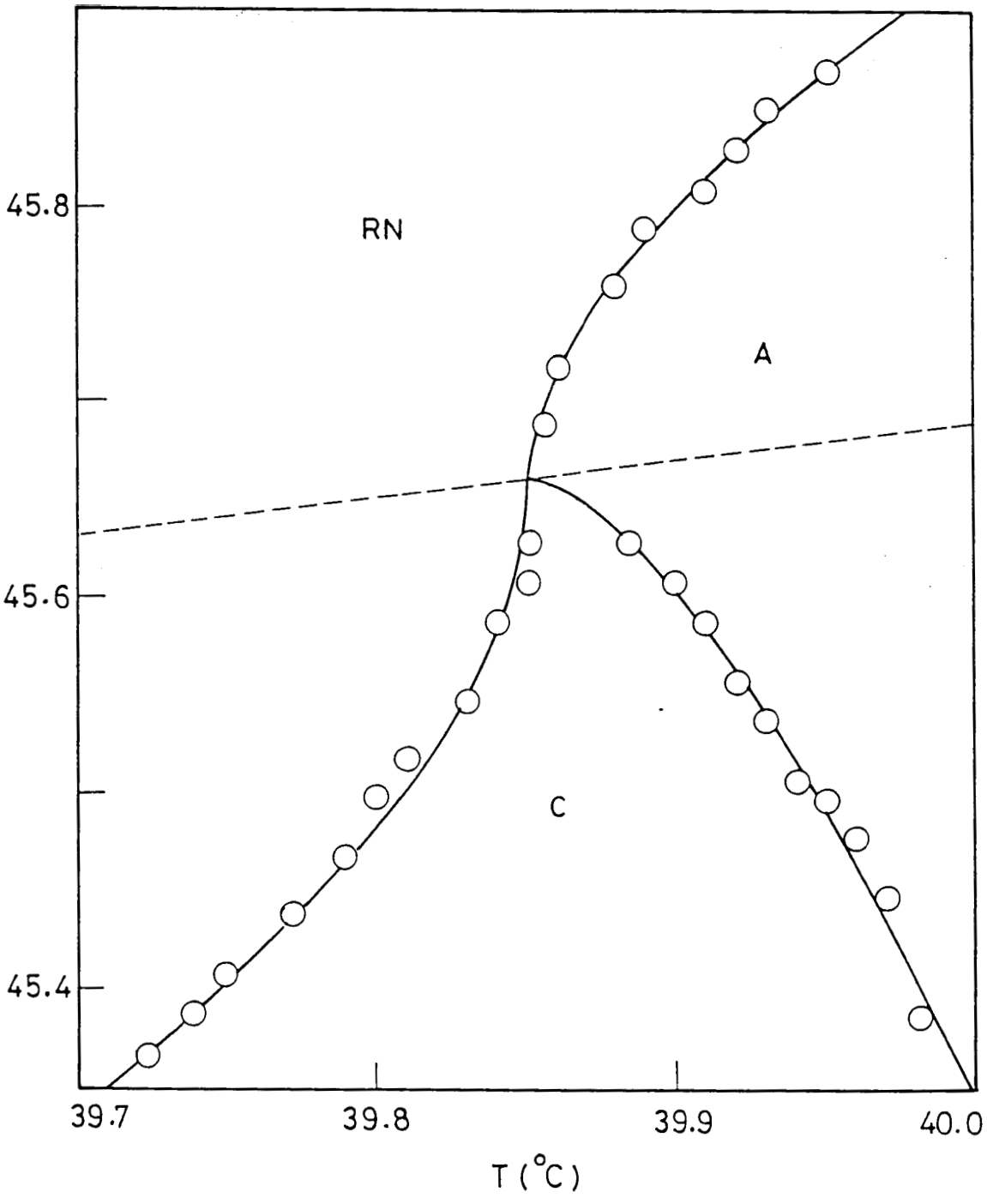

Figure 3.20

High resolution T–X diagram in the vicinity of the RN–C–A multi-critical point in the 8OPCB + CEPOOC binary system (X is mol % of CEPOOC). The solid lines are computer fits of our data to expressions for the A–RN, A–C and C–RN phase boundaries (see text). The dashed line represents the best-fit B term.

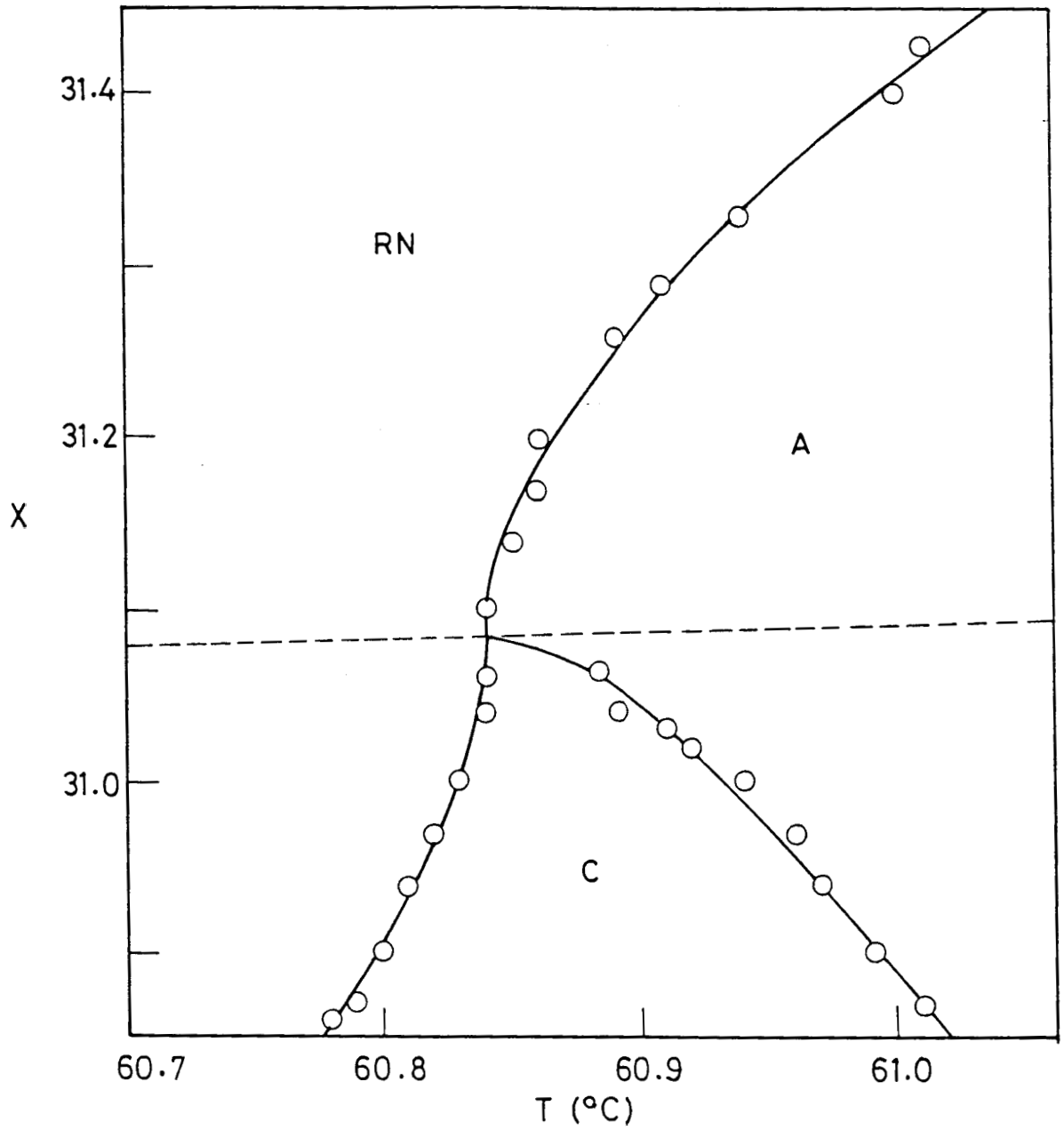

Figure 3.21

High-resolution T-X diagram in the vicinity of the RN-C-A point in the CEPDOC + CEPOOC binary system (X is mol % of CEPOOC). See also legend of Fig. 3.20.

system but with a simple 90° rotation of scaling axes. This is necessary because the sequence of transitions near the RN-C-A point is inverted compared to NAC point when the temperature is lowered, at a constant concentration. In the case of the former the nematic phase is the lowest temperature phase while in the case of latter the nematic phase occurs at the highest temperature. The expressions used by us for computations are :

$$X_{A\text{-}RN} = X_{RN\text{-}C\text{-}A} + A_{A\text{-}RN}(T_{A\text{-}RN} - T_{RN\text{-}C\text{-}A})^{\eta_{A\text{-}RN}} + B(T_{A\text{-}RN} - T_{RN\text{-}C\text{-}A}) \quad [3a]$$

$$X_{C\text{-}RN} = X_{RN\text{-}C\text{-}A} + A_{C\text{-}RN}(T_{RN\text{-}C\text{-}A} - T_{C\text{-}RN})^{\eta_{C\text{-}RN}} + B(T_{RN\text{-}C\text{-}A} - T_{C\text{-}RN}) \quad [3b]$$

$$X_{AC} = X_{RN\text{-}C\text{-}A} + A_{AC}(T_{AC} - T_{RN\text{-}C\text{-}A})^{\eta_{AC}} + B(T_{AC} - T_{RN\text{-}C\text{-}A}) \quad . \quad [3c]$$

The computations were carried out as in the case of Brisbin et al. with the universality constraint $\eta_{A\text{-}RN} = \eta_{C\text{-}RN}$, η itself being a free parameter. The values of the exponent η, the amplitude A and χ^2 for the different phase boundaries A-RN, C-RN and A-C, are given for the two binary systems in table 3.5. It is clear that the exponents η are, within statistical uncertainties, exactly same as the universal exponents associated with the NAC point.

TABLE 3.5

Best-fit parameters and values of χ^2 obtained from individual fits of our high-resolution T-X data to the expressions 3(a), 3(b) and 3(c).

	8OPCB/CEPOOC	CEPDOC/CEPOOC
B	0.20 ± 0.10	0.05 ± 0.15
T_{RN-C-A} (°C)	39.85 ± 0.01	60.84 ± 0.01
X_{RN-C-A} (mol %)	45.66 ± 0.01	31.085 ± 0.01
RN-C-A = A-RN	0.571 ± 0.03	0.569 ± 0.03
A-C	1.531 ± 0.02	1.528 ± 0.03
A_{A-RN}	0.6976 ± 0.15	0.8942 ± 0.13
A_{C-RN}	-1.0349 ± 0.20	-1.1688 ± 0.14
A_{A-C}	-6.3896 ± 0.70	-3.3215 ± 0.50
χ^2_{A-RN}	1.083	1.058
χ^2_{C-RN}	0.946	1.079
χ^2_{A-C}	1.083	0.944

Thus we have, by bringing the RN-C-A point closer in temperature scale to nematic-isotropic transition temperature, increased the experimentally observable critical region. The singularities of phase boundaries observed in the critical region have the same exponents as the NAC system proving thereby that the RN-C-A and NAC multicritical points exhibit the same universal behaviour.

3.5. SUMMARY OF CURRENT THEORETICAL AND EXPERIMENTAL UNDERSTANDING OF THE RN-C-A AND NAC MULTICRITICAL POINTS

In the light of different types of high resolution studies conducted on systems exhibiting the NAC point, it is of interest to compare the results of these studies with theoretical predictions. We shall first enumerate on the latter.

3.5.1 Theoretical Predictions

As mentioned earlier, the Chu and McMillan model was based on McMillan's microscopic theory[2] of the srnectic C phase. This theory centred around the electric dipole-dipole interactions, the dipolar orientational order bringing about the smectic A-smectic C transition. Neglecting the fluctuations in the order parameters, Chu and McMillan wrote the Landau free energy expression as

$$F = a\psi_o^2 + \frac{1}{2}b\psi_o^4 + e\beta_o^2\psi_o^2 + \frac{1}{2}f\beta_o^4\psi_o^2 \qquad [4]$$

where $\psi = \psi_o e^{(iq_z z + iq_x x)}$ is the order parameter describing the smectic layers, $\beta = \beta_o x$ is the smectic C dipolar order, and $a = a_o(T-T_1)$, $e = e_o(T-T_2)$, b and f are assumed to be positive and temperature independent.

It may be noted that in equation (4) β_o does not occur by itself in any term, but always in combination with ψ_o. This implies that the possibility of the existence of a biaxial nematic (i.e., tilt in the absence of layers, $\beta_o \neq 0$ $\psi = 0$)is ruled out. Minimising F with respect to ψ_o and β_o, the authors obtained a phase digram where the continuous NA, NC and AC phase boundaries meet at a point $T_{NAC} = T_1 = T_2$. In addition to predicting the possibility of a NAC point, they also computed the Xray structure factor in the nematic phase close to the nematic-smectic C phase transitions. The theory also found that all the three Frank elastic constants K_1, K_2 and K_3 diverge as the parallel coherence length $\xi_{||}$. This is in contrast to de Cennes's theory[26,27] where the elastic constants diverge as $\xi_{||}^{3/2}$. Apart from these, the xray scattering profile was expected to be Lorentzian throughout the nematic phase. Also, the mass density fluctuations were expected to vary smoothly across the NAC phase diagram.

In the alternative approach by Chen and Lubensky[4] the smectic C phase is induced by the tilt of the nematic director relative to the layer normal. The tilt which is an additional parameter (not an order parameter) occurs when the coefficient of the transverse gradient term becomes negative. In the ordered phase the free energy has the form

$$F = am^2 + um^4 + C_{\perp} K_{\perp}^2 m^2 + D_{\perp} K_{\perp}^4 m^4 \qquad [5]$$

where $m(r) = \int d^3 . \frac{K}{(2\pi)^3} e^{iK.r} \rho(K)$ is the scalar order parameter; $\rho(K)$ being the Fourier transform of the centre of mass density $\rho(r)$. $\rho(r)$ is periodic with the fundamental wavevectors given by q_A and q_c in the smectic A and smectic C phases respectively. In the $(C_{\perp}, T)$ space, equation (5) leads to a phase diagram with an NAC point (in Fig.3.1) at $(C_{\perp}=0, T=T_{NAC})$. All the phase transitions are continuous; however, the authors point out that owing to Brazovskii fluctuations[23] the NC transition may be driven first order.[24] The model predicts that the xray scattering intensity in the nematic phase near the NAC point falls off in the transverse direction as $q_{\perp}^{-4}$. Also, the model predicts that at the NA transition K_2 and K_3 diverge, but K_1 does not. This is in agreement with the predictions of de Gennes.[26] At the NC transition, however, the Chen and Lubensky model predicts a ξ^2 divergence for all the elastic constants which is in disagreement with the de Gennes[26] model which predicts a $\xi^{3/2}$ divergence. As stated above, at the NAC point $C_{\perp}=0$ and hence, according to the Chen and Lubensky theory, the NAC point is a Lifshitz point.[5] At this point the authors calculated that K_3 diverges as $\xi_{||}$ while K_2 and K_1 are only slightly divergent.

3.5.2. Experimental **Studies** - Phase Diagrams.

Let us now compare the topology of the NAC phase diagram obtained experimentally with those predicted by the two models.

In the first experimental phase diagram[6] ($\bar{7}S5/\bar{8}S5$ system) which exhibited a NAC point in T-X plane, the AC and NC lines (i.e., the C line) had a common slope at the NAC point while the NA line approached it obliquely. De Hoff et al.[8] pointed out that this is in disagreement with the predictions of both the theories wherein the NA and NC lines have a common tangent with the AC line coming in obliquely. However, in the later high resolution T-X diagrams of Brisbin et al.[12] and the high resolution P-T diagram of Shashidhar et al.,[14] all the phase boundaries are shown to exhibit universal singularities. The explanation given by Brisbin et al.[12] for the non-observation of such singularities in the $\bar{7}S5/\bar{8}S5$ system[6,9] (which thus is inconsistent with the universal concept) is that in this system the amplitude of the NC line divergence (A_{NC}) is very small. They also remark that the lower density of data and precision of the $\bar{7}S5/\bar{8}S5$ experiments may be the other reasons for obtaining a non-universal topology. Our results presented in this chapter show that the same universal topology associated with NAC also holds near RN-C-A as indeed expected since the phases involved in the two cases have the same symmetry.

3.5.3. High resolution xray, calorimetric and light scattering studies.

We shall now summarise the results of important high resolution xray, calorimetric and light scattering experiments which have permitted explicit comparisons with theory.

A) Xray Scattering Studies

As remarked earlier the Chen and Lubensky model defines the NAC point as that at which the coefficient of the gradient square term in the Landau-Ginzburg free energy expression becomes zero. It also predicts the NAC point to be a m=2 Lifshitz point.[5] Since it has a lower marginal dimensionality of 3 interesting fluctuation effects should occur. The Chen and Lubensky model makes the important prediction that near the NAC point the transverse mass density fluctuations should have a $q_{\perp}^{4}$ dependence rather than the conventional Lorentzian $(q_{\perp}^{2})$ behaviour. Earlier high resolution experiments[10] conducted on the NA side of the phase diagram seemed to show disagreement with this prediction.[4] It was found that the transverse mass density fluctuations are always Lorentzian. However subsequent high resolution xray studies[1,] conducted for a series of concentrations on the NC side of the phase boundary showed some interesting behaviour. It was observed that for concentrations $X > X_{NAC'}$ the scattering in the nematic phase at higher temperatures is characteristic of smectic A fluctuations while at lower temperatures the scttering was characterised by pretransitional smectic C fluctuations. Thus the predicted fluctuations cross-over from smectic A-like to smectic C-like was indeed experimentally observed in the nematic phase. It was also observed that the pretransitional smectic C scattering is highly non-Lorentzian which is in quantitative agreement with Chen and Lubensky model. On the basis of these studies it was concluded

that the Lifshitz model of Chen and Lubensky gives a good description of the critical scattering associated with the NC transition for those concentrations which are not in the immediate vicinity of the NAC point. On the other hand, in the same concentration range, the Chu and McMillan model was found to be quite unsuccessful. However, some serious discrepancies remained with regard to the predictions of the Chen and Lubensky model in the immediate vicinity of the NAC point like for instance concerning proper location of the cross-over line and the nature of the fluctuations in the close vicinity of the NAC point. All the xray diffraction studies described above were conducted on $\bar{7}S5$ and $\bar{8}S5$ system which in fact was the first system in which the NAC point was seen. Very recently, however, Martinez-Miranda et al.[28] have made high resolution xray studies of the pretransitional fluctuations above the NC phase boundary in another binary system, viz., $\bar{7}S5/8OCB$. These studies have given some extremely important results. It was found from the xray study in nematic phase that the smectic mass density fluctuations are always well described by the simple Lifshitz form proposed by Chen and Lubensky. Thus the studies by Martinez-Miranda et al. have located the Lifshitz line along which the coefficient of gradient square term of Landau-Ginzburg free energy expression vanishes. They also found the extremely interesting result; that the Lifshitz line mirrors the AC boundary (Fig.3.22). Thus on the whole the xray scattering results are in very good agreement with the Lifshitz point model of Chen and Lubensky.

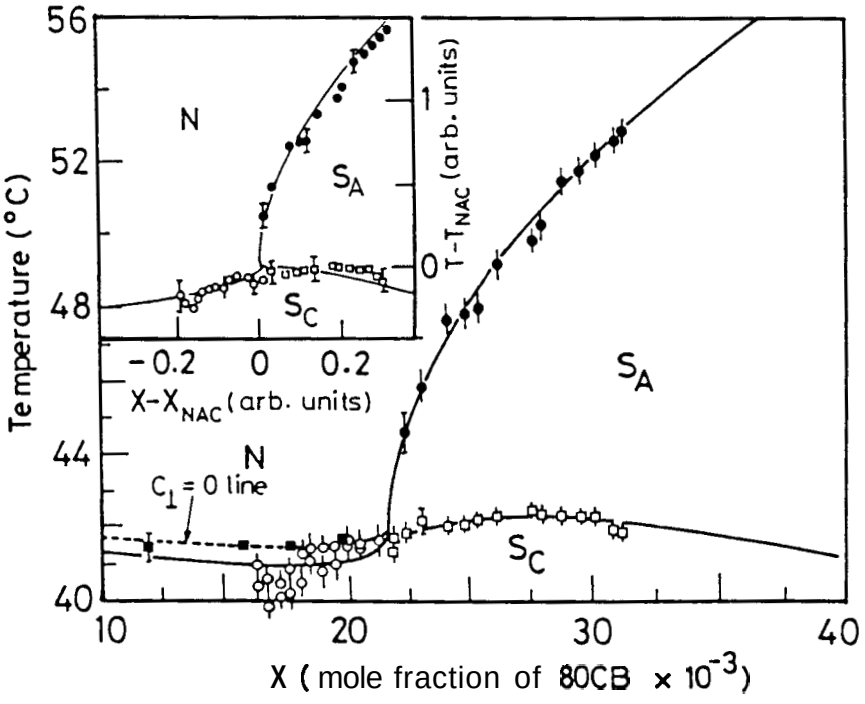

Figure 3.22

NAC phase diagram obtained from the polarising microscope studies. Solid circles, T_{NA} ; open squares, T_{AC} ; open circles, T_{NC} ; solid squares denote the fluctuation cross over points as obtained by Xray studies (see ref. 28).

B. Calorimetric studies and comments on the order of phase transitions on approaching the NAC point

The earliest calorimetric work on systems exhibiting the NAC point is due to Johnson et al.[6] on $\bar{7}S5/\bar{8}S5$ binary system. Subsequently more detailed calorimetric studies (AC calorimetry and adiabatic) have been conducted[9,29-31] on systems exhibiting NAC point. These results will be summarised in the following :

i) NA transitions

de Hoff et al.[9] and Anisimov et al[30] have studied the specific heat changes associated with the NA transitions for the $\bar{7}S5/\bar{8}S5$ system and 4-n-hexyloxy phenyl-4'-n-octyloxybenzoate/4-n-hexyloxy phenyl-4'-n-decyloxy benzoate ($\bar{6}.O.\bar{8}/\bar{6}.O.\bar{10}$) system respectively (Figs. 3.23 and 3.24). In both cases it was observed that the amplitude of the specific heat anomaly decreases rapidly as the NAC point is approached. Two alternative explanations for the disappearance of specific heat anamoly associated with the AN transition have been proposed. De Hoff et al.[9] have argued that the disappearance of the specific heat anamoly is probably not related to NAC point at all, but, could be due to an increase of smectic A bare coherence length which in turn is due to enhancement of the nematic range. The increase in bare correlation length in fact has been seen in Xray experiments.[32] Coradetski and Podnek[33] have argued that the results of Anisimov et al. and of de Hoff et al. could be explained as being due to exis-

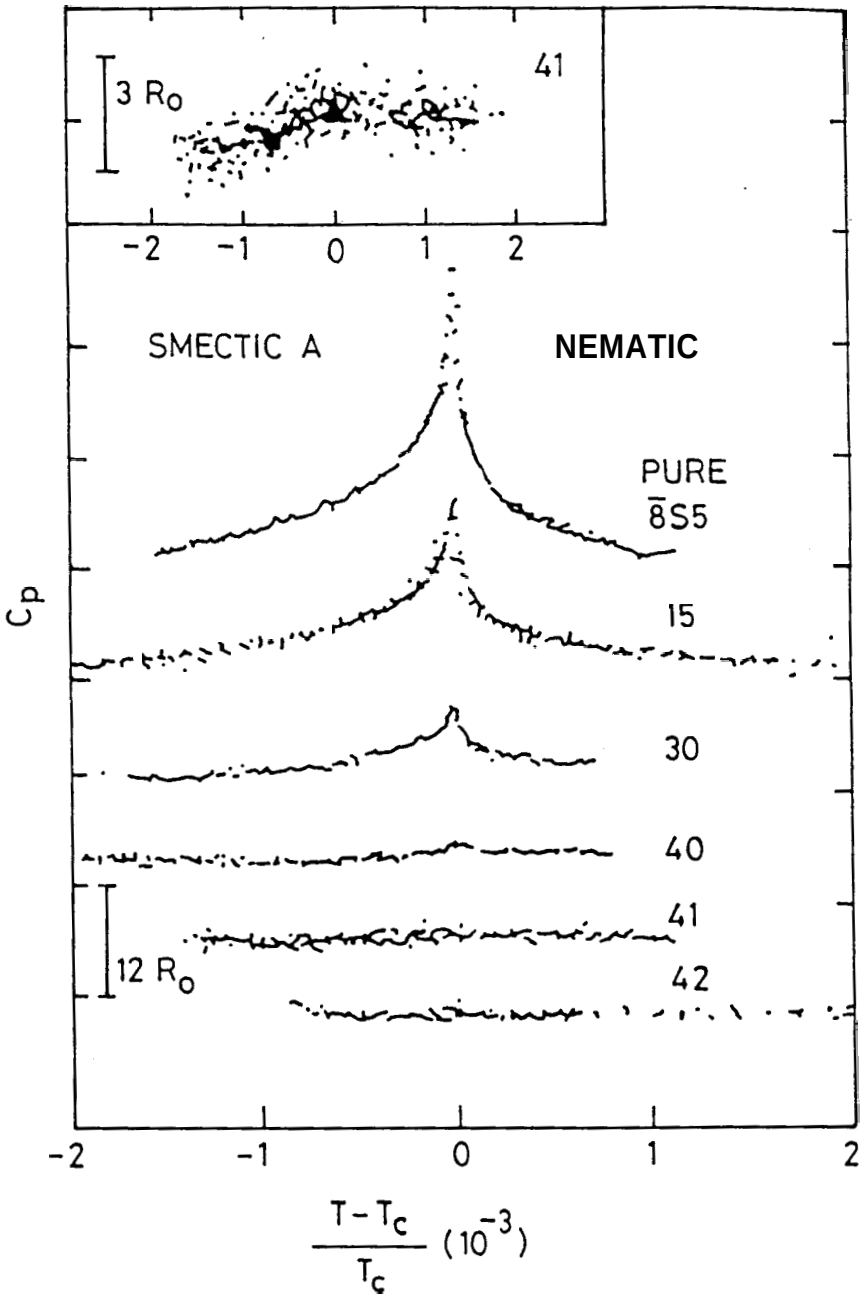

Figure 3.23

Specific heat vs. reduced tenperature at the NA transitions of pure $\bar{8}S5$ and five mixtures (15–42% $\bar{7}S5$) (ref. 9).

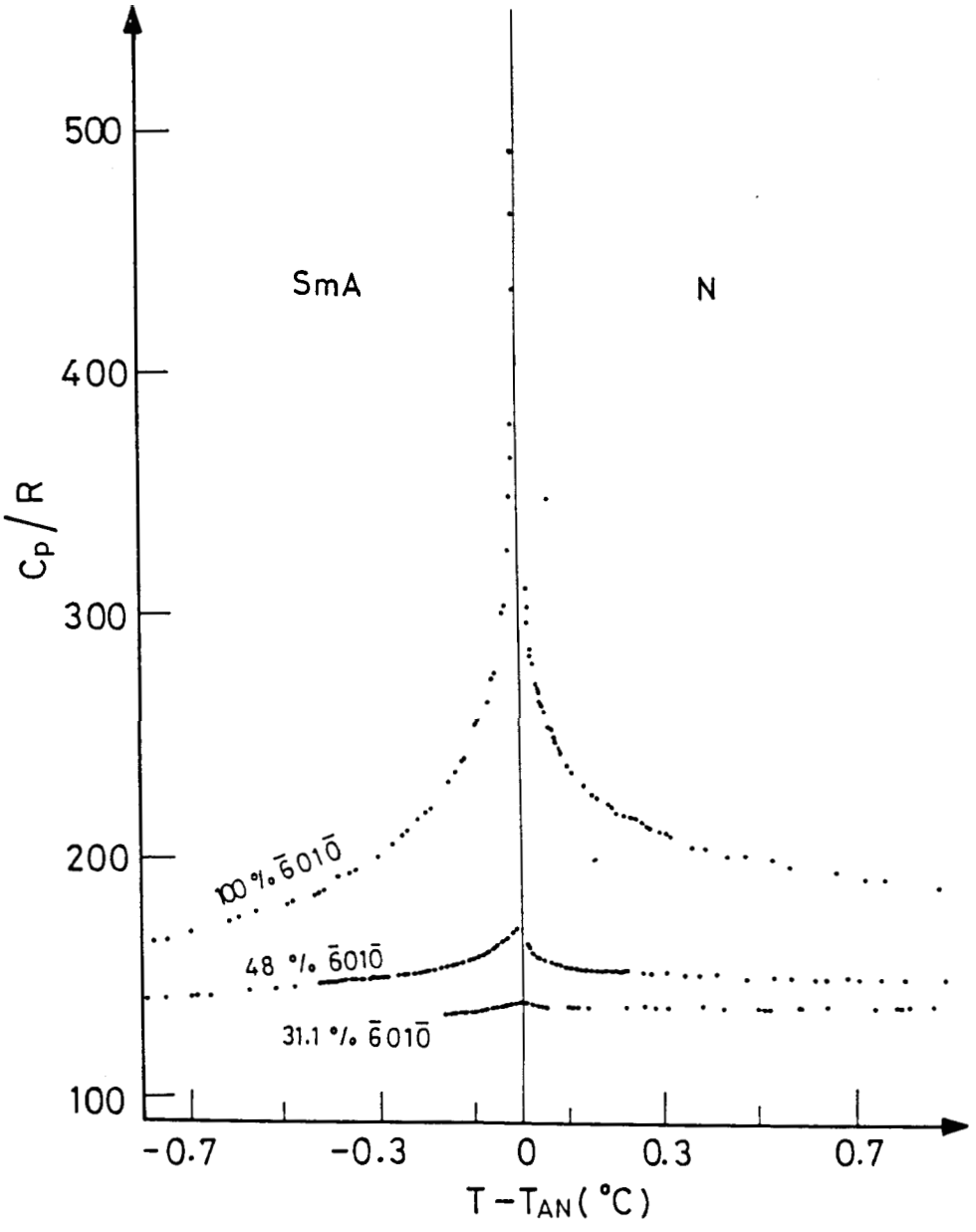

Figure 3.24

Heat capacity near the A-N transitions (ref. 30)

tence of "reentrant point" at or very close to NAC point. This theory which treats the smectic fluctuations in the Ornstein-Zernike approximation predicts a typical phase diagram for the NAC system as shown in Fig.3.25. It is interesting that the theory predicts (i) a crossover line ($Q = Q_C$ line) at which smectic A like fluctuations change to smectic C like fluctuations ($Q < Q_C$ denoting S_A like and $Q > Q_C$ denoting C like regions) and (ii) that this crossover line must be parallel to the nematic-isotropic boundary. This has not been rigorously tested in any experimental system so far.

(ii) NC transitions

There have been so far three accurate specific heat measurements on the NC line for systems exhibiting NAC point, viz., 7S5/8S5,[9] 6.O.8/6.O.10[30] and 7S5/8OCB[31] systems. Chronologically the measurements of De Hoff et al preceded the others. It was observed by them that the thermal behaviour near NC line is markedly different from that near the NA line. While the NA transitions were continuous exhibiting strong fluctuations, the NC transitions were seen to exhibit first order behaviour with very weak fluctuations (Fig. 3.26). de Hoff et al. have also evaluated the transition entropy for the NC transition using AC calorimetry and differential scanning calorimetry techniques. Such a combined technique permitted them to achieve a precision of $\pm 0.001\ R_o$ in the determination of transition entropy ΔS_{NC}. Fig.3.27 shows the plot of ΔS_{NC} versus X (concentration) of

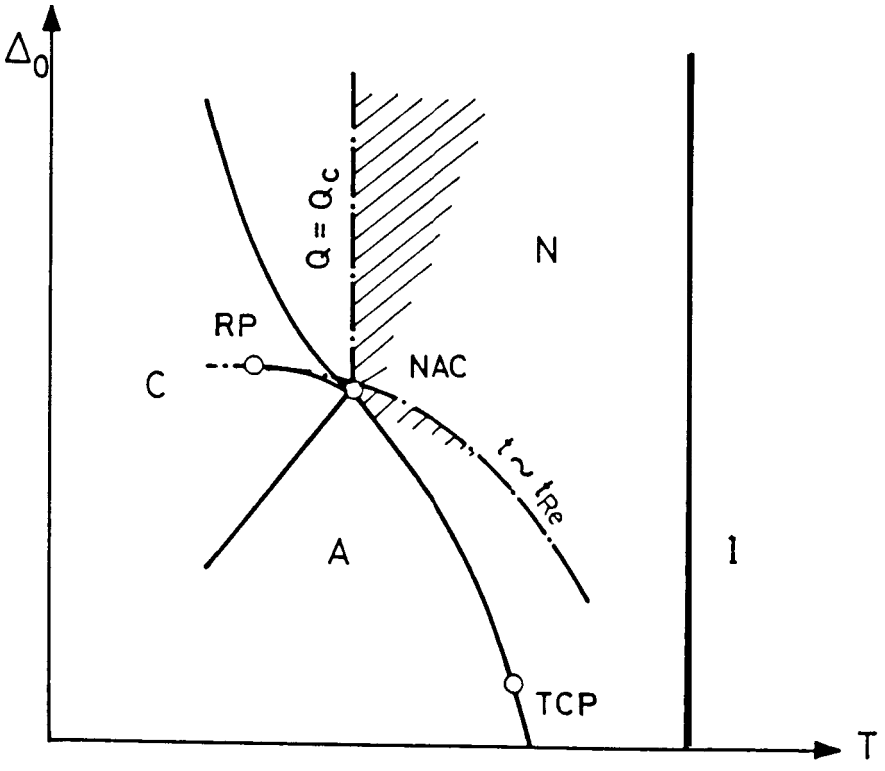

Figure 3.25

A typical phase diagram of LC. The singular points on the NA line which determine the behaviour of different quantities for $Q < Q_c$ (A regime), are indicated. The shaded region shows the region of non-Lorentzian behaviour. The figure also shows a "reentrant point" (RP) as well as a tricritical point (TCP) (Ref. 33).

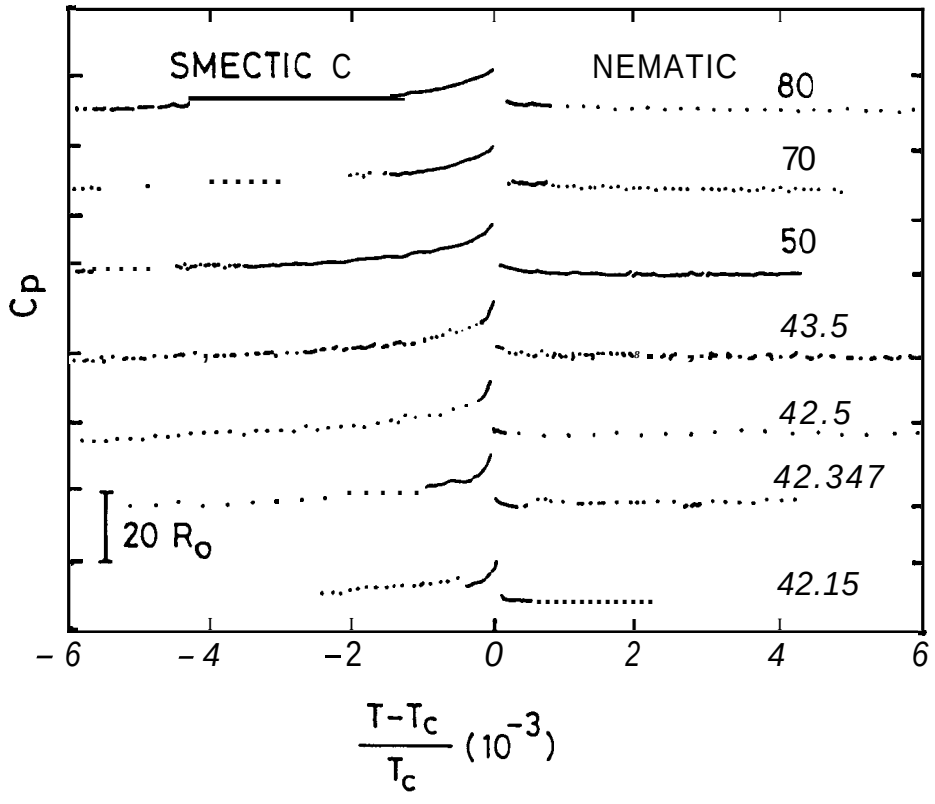

Figure 3.26

Specific heat vs. reduced temperature near the NC transition of several mixtures. The zero of the ordinate is different for each concentration of $\bar{7}S5$, 43.5 - 80%. The baseline is approximately 1100 J/mol°C in each case (Ref. 9).

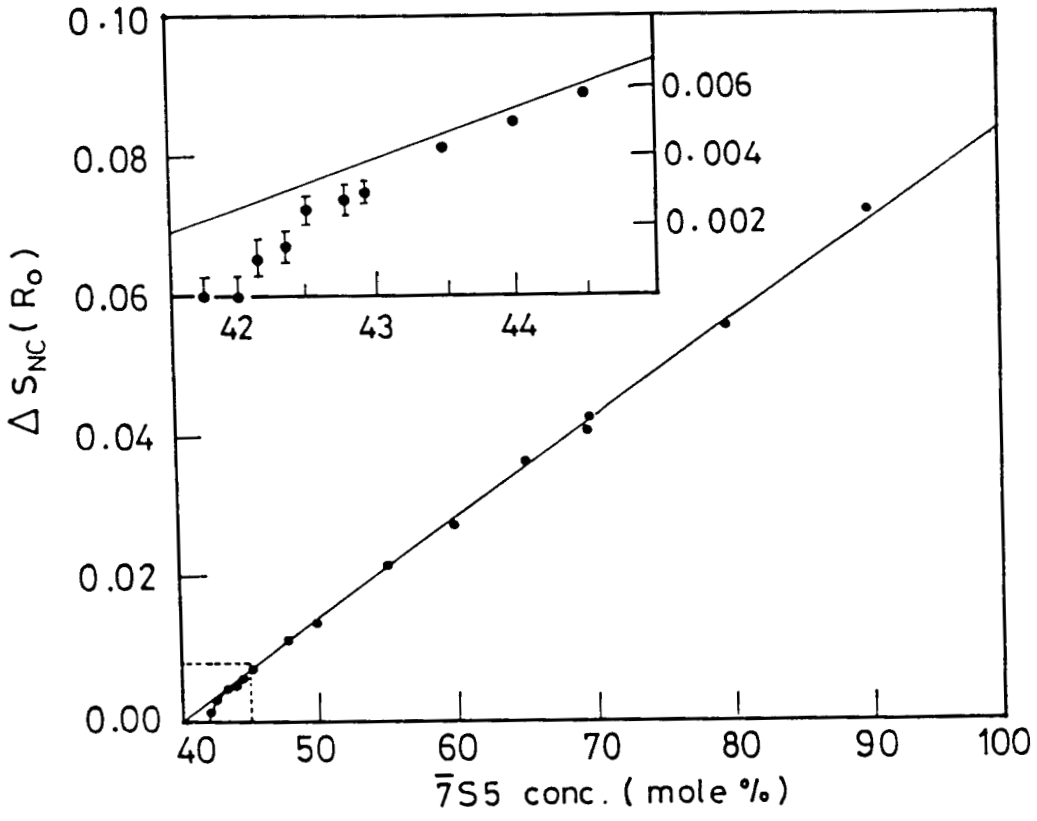

Figure 3.27

NC transition entropy versus concentration. Solid lines are fits to the data at concentrations greater than 45%. Inset is an expansion of region enclosed by dotted lines. Each point represents the average of 15 to 25 scans involving several samples (ref. 9).

7S5/8S5, determined accurately in this manner. It is clear that $(\Delta S)_{NC}$ goes to zero very close to or at the NAC point. The experimental results of Anisimov et al. are shown in Fig.3.28 and Fig.3.29. The specific heat anomoly near the NC transition for the 32.5% (mol %) mixture of 6.O.8/6.O.10, is shown in Fig. 3.28 while Fig.3.29 reproduces transition entropy for the NC transition as a function of concentration. Thus the results of both Anisimov et al. and De Hoff et al. seem to show that the entropy of NC line goes to zero at $X_{NAC'}$ the variation itself being somewhat nonlinear very close to $X_{NAC'}$

The most recent specific heat investigation of NC transition in NAC system is due to Garland and Huster[31] who have studied 1.95 mol% of 80CB in 7S5. This concentration is very close to NAC point (at 2.74 mol%). They found that their data are well described by Landau model in which the first order nature of transition is very weak. Thus they concluded that there should be a classical Landau tricritical point for the NC transition at or very close to the NAC point.

(iii) AC transition

The specific heat[9] data on AC transitions in 7S5/8S5 system are shown in Fig.3.30. This appears to be the most exhaustive specific heat study of AC line for a NAC system. Weak fluctuation contributions are seen to characterise these transitions. To this extent the specific heat behaviour of AC transition resembles that of NC

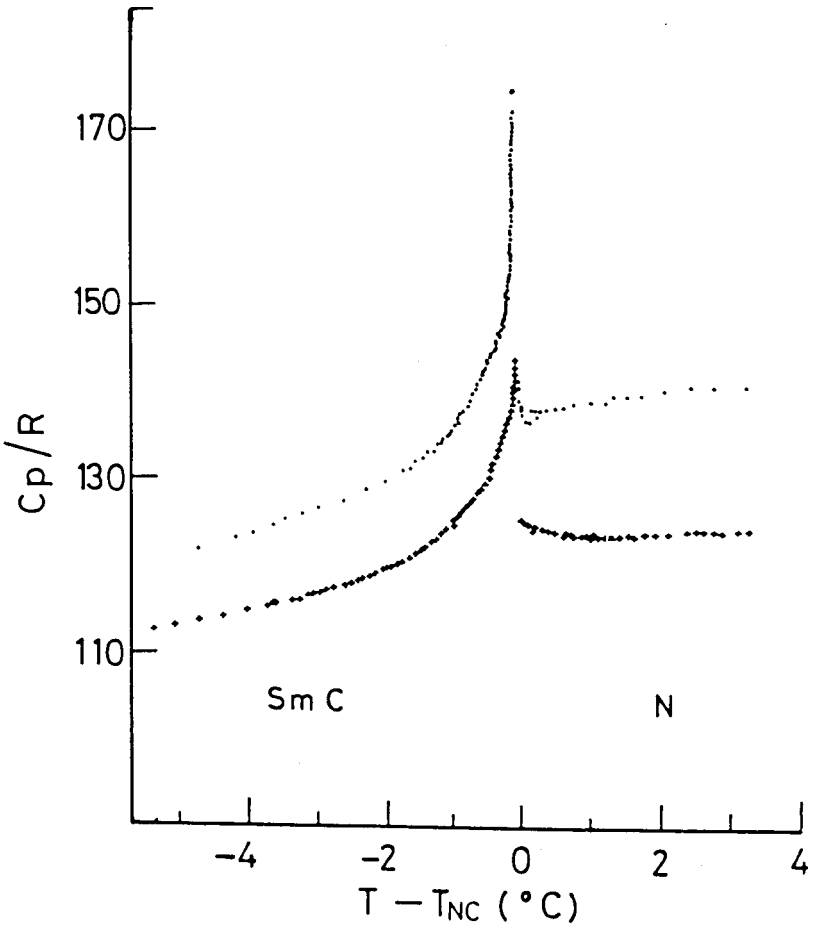

Figure 3.28

Heat capacity near the N-C transition in the pure 608 (crosses) and 32.5% mixture (dots) (ref. 30).

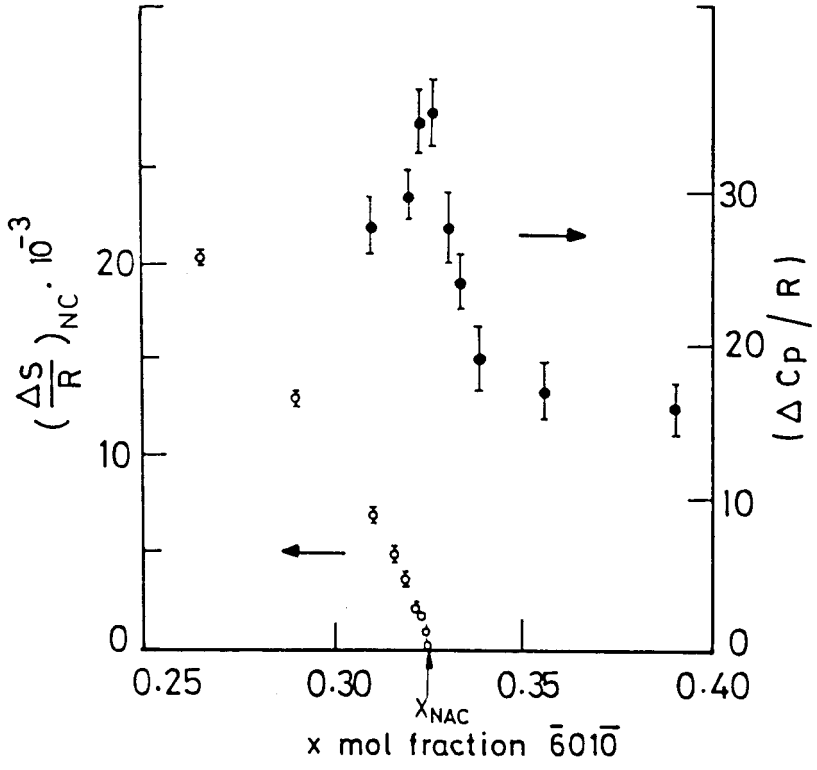

Figure 3.29

N–C transition entropy and heat capacity jumps near the NAC point (ref. 30).

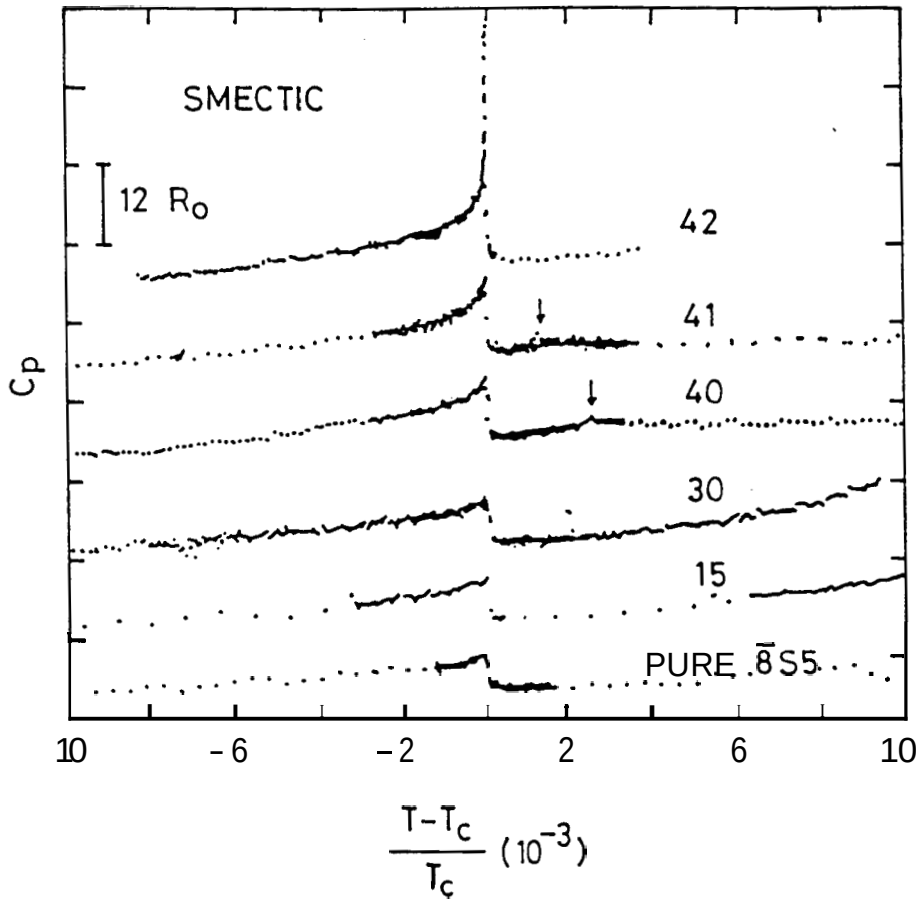

Figure 3.30

Specific heat vs. reduced temperature near the AC transitions of pure $\bar{8}$S5 and five mixtures (15-42% $\bar{7}$S5). The arrows designate NA transitions. The 42% sample is very close to the NAC point (ref. 9).

transition while it appears to be different from that of NA transition. A comparison of magnitudes of specific heat jumps (ΔC_P) along the C line shows that while AC_P associated with the NC transition is constant (to within experimental conditions) for all concentrations up to NAC point (see Fig. 3.26), AC_P for AC diverges sharply as the NAC point is approached, this being more pronounced for concentrations very close to X_{NAC} (Fig.3.30). The analysis of this data also appears to show that for all concentrations the AC line can be described as mean field behaviour. Anisimov et al.[29] have argued that the NAC point could also be a tricritical point for the AC line.

In summary the calorimetric data seem to indicate that while NA is truly second order right up to NAC point, the NC transition which is first order away from the NAC point, is likely to have a tricritical point at or very close to NAC point. The possibility that the AC line could also have a tricritical point at the NAC point cannot be ruled out. Evidently, further studies are required to prove these points.

c) Light Scattering Studies

The first detailed light scattering experiment near NAC point is due to Witanachi et al.[34] who studied the behaviour of bend elastic constants above the NC transition in $\bar{7}S5/\bar{8}S5$ system. They found that the nature of director fluctuations in $\bar{7}S5/\bar{8}S5$ mixtures indicate that the NC transition near the NAC point exhibits both smectic layer and tilt fluctuations. These results cannot be adequately descri-

bed by any of the existing models. Solomon and Litster[35] have reported light scattering measurements of nematic director fluctuations near the NAC point in the 7S5/8S5 system. They were able to analyse the data and correct for the effects of curvature of phase boundary and elucidate the evolution in the critical behaviour as the NAC point is approached both from the NA and NC sides of the multicritical point. Their results on NA and NC boundaries are represented in Fig.3.31 and Fig.3.32. A notable feature of the data on NA transitions is the increase in correlation length as NAC point is approached. As remarked earlier (see section 3.5.1), the different theoretical models make different predictions concerning the behaviour of K_1 and K_2 at the Lifshitz point and along NC line. However they all predict a similar divergent behaviour of K_3 along the NA line. The data of Solomon and Litster are consistent with predictions of Chen and Lubensky model for Lifshitz point and NA lines. Perhaps, the most striking feature of the data of Solomon and Litster is the increase of K_3 to a maximum value at a temperature above that of NC transition and its decrease as the transition is approached. This behaviour is also clearly visible in the Xray measurements of Martinez-Miranda[28] shown in Fig.3.33. It must also be remarked that more recent experiments of Huang and Ho[36] who have determined bend elastic constants near NAC point by Freedericksz technique have also shown a similar behaviour for K_3. This effect is however not anticipated by any of the existing models and therefore needs to be addressed to theoretically.

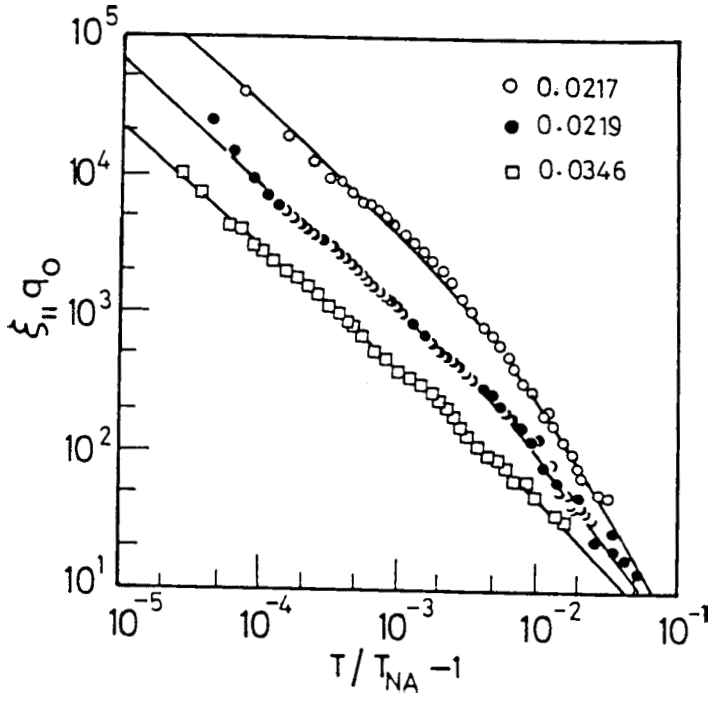

Figure 3.31

$\xi_{\parallel} q_0$ in the N-A samples. The key gives the mole fraction of 80CB in the mixtures (ref. 35).

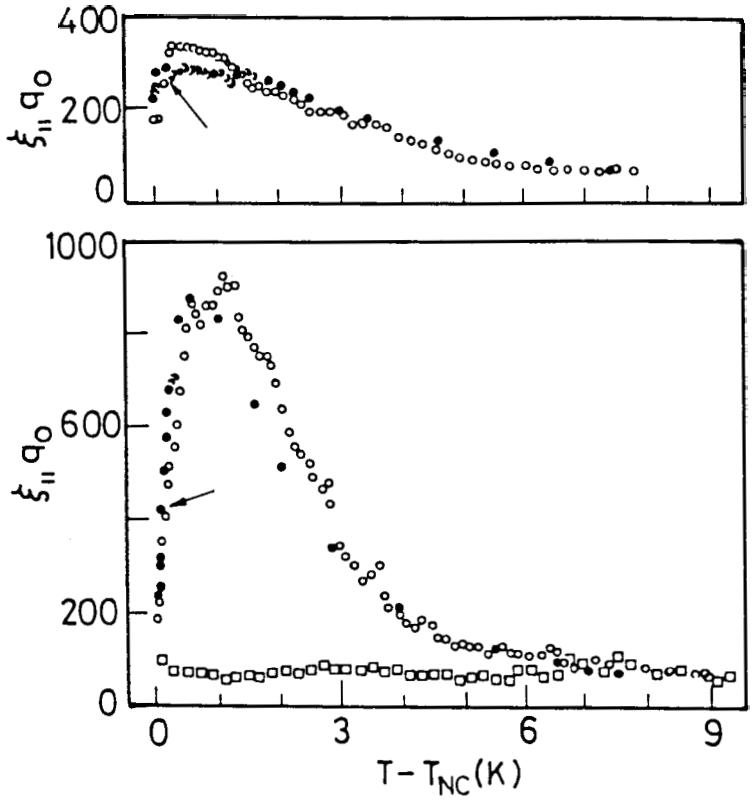

Figure 3.32

Nematic phase behaviour in the N-S_C samples. The open circles are the light-scattering (inverse intensity) data which have been scaled to agree with the Xray results at $T > T_{NC} + 6$ K, and the solid circles are the X-ray data measured at $q_{\perp} = 0$. The arrow indicates the Lifshitz line. The upper panel is the $X_{80CB} = 0.0176$ sample, and the lower panel is the 0.0197 sample. The square symbols in the lower panel are the K_2 data points (ref. 35).

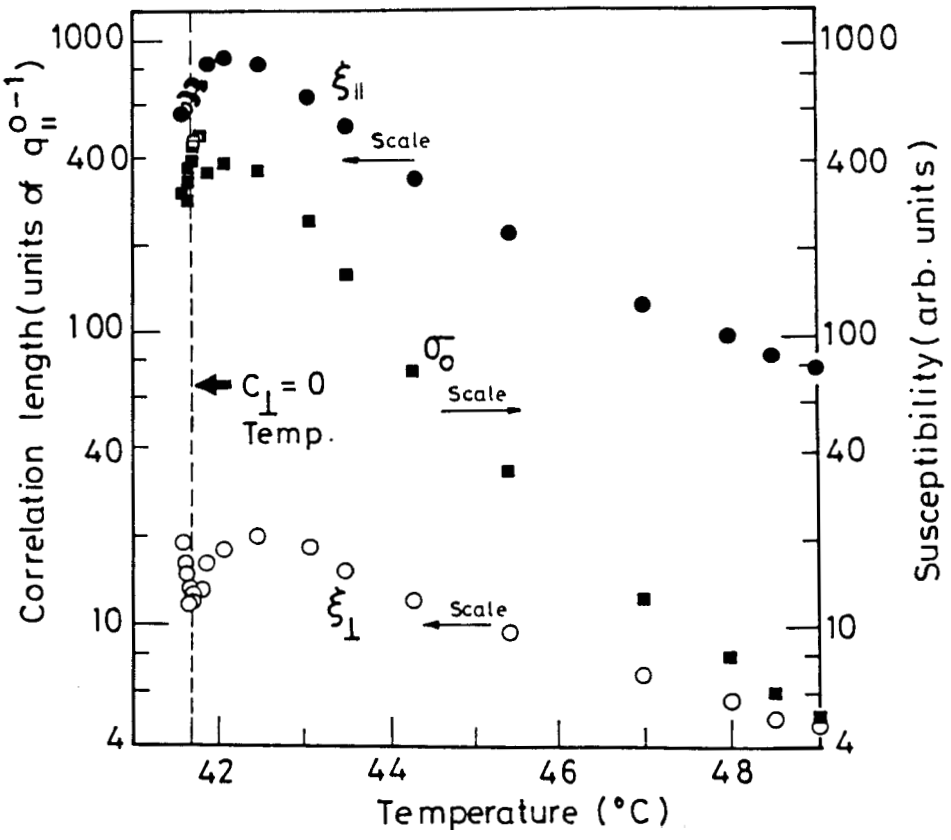

Figure 3.33

Susceptibility, longitudinal and transverse correlation lengths as obtained by Xray scattering studies for the $X_{8OCB} = 0.0197$ sample ; $q_{\parallel}^{o} = 0.23195\ \mathring{A}^{-1}$ (ref. 28).

3.5.4. Disloction loop theory of NAC point

Grinstein and Toner[37] have applied the renormalization group technique and developed a dislocation loop theory of NAC point in three dimensions. The theory makes some important predictions:- Four (rather than three) phases are predicted to meet at a point where AN and AC phase boundaries cross (Fig.3.34). The new phase, a biaxial nematic (N') intervenes between C and N phases and is supposed to be intermediate between them in properties. It exhibits the orientational long range order of C phase; that is, the smectic layers are tilted in a fixed direction relative to the nematic director. The translational properties of N' are supposed to be that of the nematic, i.e., the layers are expected to have only short range positional order in contrast to C phase which possesses quasi long-range positional layered order. Thus sufficiently close to NAC point, NC transition, which is first order far from this point and is characterized by simaltaneous onset of long range orientational and quasi long-rang? positional order, is predicted to occur in two stages through the N' phase. The system acquires orientational long range order at the NN' transition and quasi long-range positional. order at the CN' transition. Both these transitions are continuous. N' is therefore a three dimensional analog of 2D hexatic phase which sometimes separates 2D solid and liquid states, allowing a two-stage, continuous melting process. The theory also predicts that the phase boundaries pass through this point unaffected, i.e., the AC and NN' boundaries form

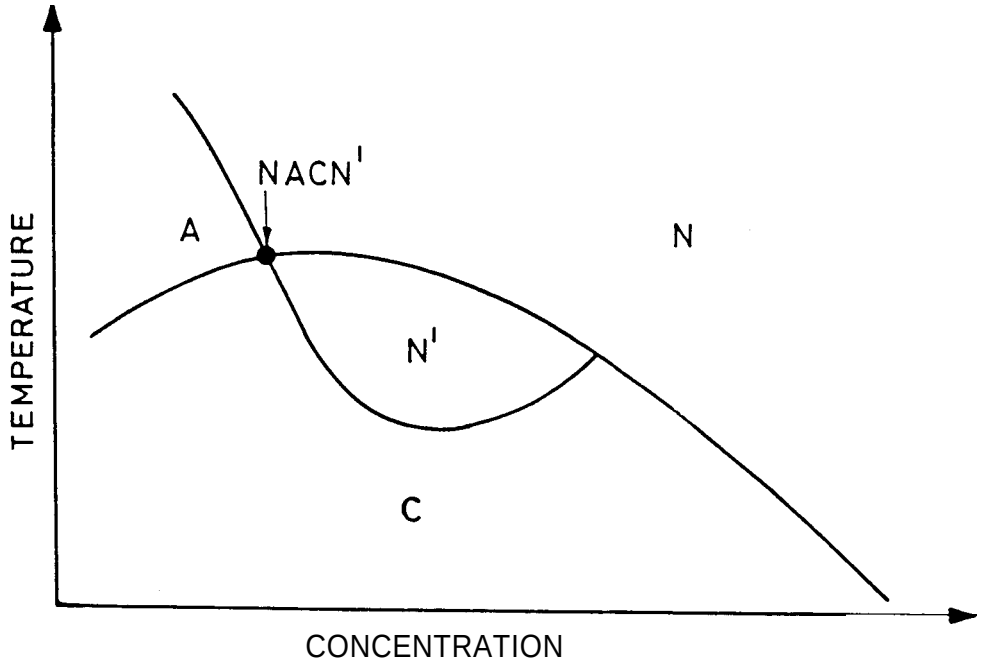

Figure 3.34

Phase diagram predicted by the dislocation-loop theory. Its crucial feature is the NACN' point which replaces the NAC point (ref. 37).

a single continuous curve through the NACN' point while AN and CN' lines should also do the same. The critical properties of NACN' point are therefore a simple superposition of those of the AN and AC transitions and fall respectively into the universality class of inverted XY transitions and simple xy transitions. In the language of magnetic systems, the NACN' point is therefore a decoupled tetra-critical point.

However none of the experiments on single component systems or mixtures, using techniques as varied as calorimetry, xray and light scattering, have shown any evidence of existence of N' phase. Thus the dislocation loop theory has failed to bring experiments and theory close to each other.

It should also be pointed that although it is now well established that the topology of the phase diagram near the NAC and RN-C-A points exhibits the same universal behaviour, there is as yet no theory which explains as to why this should be so.

In summary more work is required to be carried out for a complete understanding of the NAC multicritical point. A study of the systems exhibiting the RN-C-A point is also very important. Apart from the phase diagrams discussed in this chapter no high resolution work seems to have been done on any system exhibiting RN-C-A point. It is interesting to note from high resolution phase diagrams (Figs. 3.20 and 3.21) that, these systems are probably ideally suited

for an accurate study of the multicritical point. The reason for this is the following: Generally, considering the topology of NAC point (Fig. 3.4), the NA line has a very steep curvature close to NAC point, and to probe the fluctuation behaviour very close to NAC point one would have to go almost tangentially to NA boundary to study any parameter as a function of temperature at a constant concentration. The topology of the RN-C-A system (Figs. 3.20 and 3.21) with a 90° rotation of the experimental scaling axes simplifies this problem because one can now approach NAC point from the nematic side without having to worry about strong curvature of phase boundaries. Thus such systems are in fact ideally suited for a careful study of the biaxial fluctuations or of the possible existence of the biaxial nematic extremely close to the multicritical point. Such experiments are being undertaken[38] and should throw further light for a clear understanding of this interesting multicritical point.

REFERENCES

1 K.C.Chu and W.L.McMillan, Phys. Rev. A15, 118 (1977)

2 W.L.McMillan, Phys. Rev. **A8**, 1921 (1973)

3 K.K.Kobayashi, Phys. Lett., **31A**, 125 (1970); W.L.McMillan, Phys. Rev. A4, 1238 (1971); P.G.de Gennes, Solid State Commun., 10, 753 (1972).

4 J.H.Chen and T.C.Lubensky, Phys. Rev. **A14**, 1202 (1976).

5 R. M.Hornreich, M.Luban and S.Shtrikmann, Phys. Rev. Lett. 35, 1678 (1975).

6 D.Johnson, D.Allender, R. De Hoff, C.Maze, E.Oppenheim and R.Reynolds, Phys. Rev. **B16**, 470 (1977).

7 G.Sigaud, F.Hardouin and M.F.Achard, Solid State Commun. 23, 35 (1977).

8 R. De Hoff, R. Biggers, D. Brisbin, R.Mahmood, C.Gooden and D. L. Johnson, Phys.Rev.Lett. 47, 664 (1981)

9 R. De Hoff, R. Biggers, D. Brisbin and D.L.Johnson, Phys.Rev. A25, 472 (1982).

10 C.R.Safinya, R.J.Birgeneau, J.D.Litster and M.E.Neubert, Phys. Rev.Lett. 47, 668 (1981)

11 C.R.Safinya, L.J.Martinez-Miranda, M.Kaplan, J.D.Litster and R.J.Birgeneau, Phys. Rev. Lett. 50, 56 (1983).

12 D.Brisbin, D.L.Johnson, H.Fellner and M.E.Neubert, Phys. Rev. Lett. 50, 178 (1983).

13 R.Shashidhar, A.N.Kalkura and S.Chandrasekhar, Mol. Cryst.Liq. Cryst.Lett. 64, 101 (1980).

14 R.Shashidhar, B.R.Ratna and S.Krishna Prasad, Phys. Rev. Lett. 53, 2141 (1984).

15 D. L. Johnson (Private communication)

16 R.Shashidhar, A.N.Kalkura and S.Chandrasekhar, Mol. Cryst.Liq. Cryst.Lett. 82, 311 (1982).

17 For details of high pressure cell, see, A.N.Kalkura, "High Pressure Studies of Liquid Crystals", Ph. D. Thesis, University of Mysore (1982).

18 W. Weissflog, G.Pelzl, A. Wiegelben and D.Demus, Mol. Cryst.Liq. Cryst.Lett. 56, 295 (1980).

19 R.Shashidhar, S. Krishna Prasad and S.Chandrasekhar, Mol. Cryst. Liq. Cryst. 103, 137 (1983).

20 G.Sigaud, Y.Guichard, F.Hardouin and L.G.Benguigui, Phys. Rev.A26, 3041 (1982).

21 G.Pelzl, S.Diele, A. Wiegelben and D.Demus, Mol. Cryst.Liq. Cryst.Lett. 64, 163 (1981); G.Pelzl, U.Bottger and D.Demus, Mol. Cryst.Liq. Cryst. 64, 283 (1981).

22 L.P.Kadanoff, in Critical Phenomena, Enrico Fermi Course LI, Ed. M.S.Green (Academic, New York, 1971) p.100.

23 S.A.Brazovskii, Zh. Eksp.Teor.Fiz.**68**, 175 (1975) (Sov.Phys. JETP 41, 85 (1975).

24 J.Swift, Phys.Rev.**A14**, 2274 (1976).

25 See e.g., J.D.Litster and R.G.Birgeneau, Phys.Today **35**(5), 26 (1982).

26 P. G. de Gennes, Mol. Cryst. Liq. Cryst., 21, 49 (1973)

27 See also D.L.Johnson, J. Chim. Phys., 80, 45 (1983)

28 L.J.Martinez-Miranda, A.R.Kortran and R.J.Birgeneau, Phys. Rev.Lett. 56, 2264 (1986).

29 M.A.Anisimov, V.P.Voronov,A.O.Kulkov and F.Kholmurdov, JETP Lett. **41**(6), (1985).

30 M.A.Anisimov, V.P.Voronov, A.O.Kulkov and F.Kholmurdov, J.Phys. (Paris), 46, 2137 (1985)

31 C.W.Garland and M.E.Huster, Phys.Rev.A, Rapid Communications 35, 2365 (1987)

32 C.R.Safinya (Private communications).

33 E.E.Gorodetskii and V.E.Podnek, JETP Lett. **39**(11), June 1984.

34 S. Witanachi, J.Huang and J.T.Ho, Phys.Rev.Lett. 50, 594 (1983).

35 L.Solomon and J.D.Litster, Phys.Rev.Lett. 56, 2268 (1986).

36 Juyang Huang and John T. Ho, Phys.Rev.Lett. 58, 2239 (1987).

37 G.Grinstein and John Toner, Phys.Rev.Lett. 51, 2386 (1983).

38 D.Cohen, R.Shashidhar and J.D.Litster (Private communications).